MOLECULAR DYNAMICS STUDIES OF SUPERIONIC CONDUCTORS

Yutaka Kaneko

May 1989

MOLECULAR DYNAMICS STUDIES OF SUPERIONIC CONDUCTORS

Yutaka Kaneko

May 1989

ABSTRACT

Dynamics of diffusion and its relation with the interionic potential in superionic conductors are studied with use of the molecular dynamics method. The model systems for α-AgI and CaF_2 are analyzed from the following viewpoints. First we investigate the characteristics of the interionic potential which give rise to the superionic phase. Secondly we investigate dynamic correlations and the mechanism of diffusion. The difference in the diffusion mechanism between α-AgI and CaF_2 is studied in detail. The interionic potential is assumed to consist of the Coulomb and the soft-core potentials. The system has a simple scaling property and the thermodynamic state is characterized by the ratio of core radii, the ratio of the Coulomb potential to the soft-core potential and the reduced temperature.

In α-AgI we outline the region in scaling parameters in which I^- ions form a stable bcc lattice and Ag^+ ions diffuse with a high mobility. The results are interpreted in view of the scaling law. It is shown that Pauling's concept of the additivity rule of ionic radii is necessary for the stability of the I^--sublattice and the Coulomb force must be appropriately weak for the diffusion of Ag^+ ions to take place. The dynamic correlations between Ag^+ and the I^--sublattice are studied in detail The characteristics of

the driving force of diffusion are examined. The collective motions are investigated by calculating dynamical structure factors and current correlation functions. It is shown that the vibrational motions of Ag^+ and I^- are strongly correlated in the longitudinal acoustic mode at long wavelengths. The motion of Ag^+, however, has no correlation with the longitudinal optic mode of the I^--sublattice for large wave vectors. Summarizing these results, the diffusion mechanism of Ag^+ ions is presented from a dynamical viewpoint.

In CaF_2 we investigate the dependence of the distribution of F^- ions on the interionic potential. It is found that the diffusion path is largely influenced by the softness of the soft-core repulsion. Dynamical properties of CaF_2 are studied in comparison with those of α-AgI. The jump diffusion picture of F^- ions so far discussed in earlier works is reconfirmed in the present study. In contrast with the case of α-AgI, the diffusion of F^- occurs by strongly correlated hops between well defined sites. We further study the dynamics of the correlated jumps. Our data suggest that there are two types of motions in a sequence of successive jumps of F^- ions. A new mechanism of the correlated jumps is discussed.

ACKNOWLEDGMENTS

The author would like to express his sincere gratitude to Professor Akira Ueda, Kyoto University, for his guidance and discussions through the years of investigations. He is also grateful to Mr.Atsuo Fukumoto, Toyota Central Research and Development Labs., Inc., and Mr.Mitsuhiko Hokazono, Mitsubishi Electric Corporation, for their valuable advice and assistance in carrying out the computations. He wishes to express his gratitude to Professor Yasuaki Hiwatari, Kanazawa University, Dr.Toyonori Munakata and Dr.Akito Igarashi, Kyoto University, for useful discussions.

The author is indebted to the computer center of the Institute of Plasma Physics, Nagoya University, at which main computations were performed. Computations were also made on the computer of the Data Processing Center, Kyoto University.

CONTENTS

CHAPTER I

INTRODUCTION

Superionic conductors(SIC's) are solid state systems which exhibit a high ionic conductivity well below their melting point. Most of the ordinary solids show the ionic conductivity of the order of $10^{-8}\Omega^{-1}cm^{-1}$ at moderate temperatures. SIC's are characterized by the ionic conductivity more than $10^{-3}\Omega^{-1}cm^{-1}$, and in some class of materials the conductivity reaches values of the order of 1 $\Omega^{-1}cm^{-1}$, which are typical of those found in molten salts or ionic solutions. Carrier ions, which may be cations or anions, can diffuse with a high mobility through the lattice formed by other ion species.

The first experimental research for SIC's may be that of Tubandt and Lorentz[1] in 1914. They found that AgI displays a remarkably high ionic conductivity in the high temperature α-phase. This is due to the disorder in the Ag^+-sublattice and the distribution of Ag^+ in α-AgI and α-Ag_2S was examined by Strock[2] and Rahlfs[3] using the X-ray diffraction method. The structural properties and the phase transitions of various Ag- and Cu-conductors were investigated in the 1930's. However, SIC's were not paid further attention until the late 1960's, because Ag compounds are not suitable for practical use. The recent research for the physics of SIC's was stimulated by the work of Yao and Kummer who found the superionic conductivity in the alkali metal conductor Na β-alumina.[4] After that, many kinds of alkali metal and oxygen conductors were discovered and

applied to electronic devices such as solid state batteries and sensors. In the 1970's experimental studies of SIC's were performed extensively by the sophisticated techniques such as neutron scattering, EXAFS, infrared and Raman spectroscopy and NMR. The main results of these works are summarized in review articles.[5-8)]

SIC's are classified into three classes according to their types of the phase transition from a low temperature insulating phase to a high temperature superionic phase.[9)] In the first type(type I) there is a well defined first order phase transition which accompanies the structural change of the immobile ion sublattice. AgI- and CuI-type conductors belong to this type. In the second type(type II) there is no structural change and the conductivity gradually increases with temperature accompanying a specific heat anomaly, which resembles the λ anomaly of the second order phase transition. The SIC's with a fluorite structure such as CaF_2 belong to this type. In the third type(type III) there is no structural change and no anomaly in the specific heat. The conductivity exhibit an exponential growth with temperature. Alkali metal β-alumina is the representative of this type.

The fundamental problem in the physics of SIC's is 'why carrier ions can diffuse with a high mobility through a host lattice?'
SIC's involve both the solid-like aspect of immobile ions and the liquid-like aspect of mobile ions in one phase.

These two properties must be correlated with each other and such a correlation is expected to play an important role in the conduction processes. There are many theoretical works trying to explain the conduction mechanism in SIC's. Huberman and Martin [10] proposed the hydrodynamic theory for the coupled crystalline-cage charged-liquid fluctuations. Hinkelman and Hubermann[11] applied the small polaron theory to the dynamics of mobile ions so as to take the interaction between mobile and immobile ions into account. Yokota[12] proposed the caterpillar mechanism to analyze the correlated jumps of mobile ions. The Brownian motion in a periodic potential was extensively studied as a model of SIC's.[13] This approach was initiated by Fulde *et al.*[14] who calculated the frequency dependent mobility with use of Mori's continued fraction method.[15] Lattice dynamics studies were also performed to analyze the observed spectra of the inelastic neutron scattering[16] and the Raman scattering.[17] For SIC's, however, the theoretical treatments are rather difficult because of a high degree of disorder, the anharmonicity in lattice vibrations and the long range nature of the interaction potential. For this reason, in spite of many attempts, the theory to explain the conduction mechanism in SIC's is not constructed yet.

The molecular dynamics(MD) method is a powerful tool to study many body problems in condensed matter systems.[18] The advantage of the MD method is that physical properties of

the system with a given interaction potential is investigated without any approximations. Moreover, the experimentally inaccessible data can be obtained in MD simulations. The pioneering MD work is that of Alder and Wainwright,[19] who studied the solid-fluid phase transition of a hard-core system. Dynamical as well as structural properties of simple liquids were investigated by Rahman[20,21] and the Orsay group.[22-24] Their results showed that the experimental data such as neutron scattering spectra can be realized even by a simple interatomic potential such as a Lennard-Jones potential. The first MD study of a charged system may be due to Hansen *et al.*[25] on the dynamical properties of a classical one component plasma(OCP). Ever since their work, a lot of MD simulations have been performed for molten salts,[26-28] ionic solids,[29] binary ionic mixtures[30] and so on.

In this article we study the superionic conductivity with use of the MD method. The purpose of this thesis is to clarify the characteristics of SIC's from the following viewpoints.

(1) What are the characteristics of the interionic potential which give rise to the superionic phase?

We investigate the interrelation between the superionic conductivity and the interionic potential to find out which part of the potential is responsible for a high ionic conductivity and the stability of the sublattice.

(2) What is the mechanism of the diffusion of mobile ions?

We investigate the dynamic correlation between mobile and immobile ions and that among mobile ions to clarify the mechanism of diffusion from a dynamical viewpoint.

Two materials, α-AgI and CaF_2, are investigated. α-AgI is a prototype of the SIC of type I. Iodine ions form a loosely-packed bcc lattice and Ag^+ ions are disordered. The recent neutron diffraction study[31] showed that Ag^+ ions are distributed over the 12(d) sites in the bcc structure. (Fig.1.1) The number of the sites is six times as large as that of Ag^+ ions and the density distribution of Ag^+ extends continuously to the neighboring sites. It has been considered that Ag^+ ions move rather freely through the I^--sublattice. On the other hand, CaF_2, which is a prototype of the SIC of type II, is structurally quite different from α-AgI. Calcium ions form a closely-packed fcc lattice and fluorine ions occupy tetrahedral sites.(Fig.1.2) The ionic conduction is due to the disorder in the F^--sublattice. According to the recent experimental works,[32,33] F^- does not occupy octahedral voids in the superionic phase and diffuse among tetrahedral sites. If this picture is allowed, there is no empty site for diffusing F^- ions. Therefore the diffusion mechanism in CaF_2 is expected to be different from that in α-AgI. We study our problem (1) mainly for α-AgI. The problem (2) is studied for both α-AgI and CaF_2 and the difference between two materials is discussed.

One of the important problems in the MD simulation is

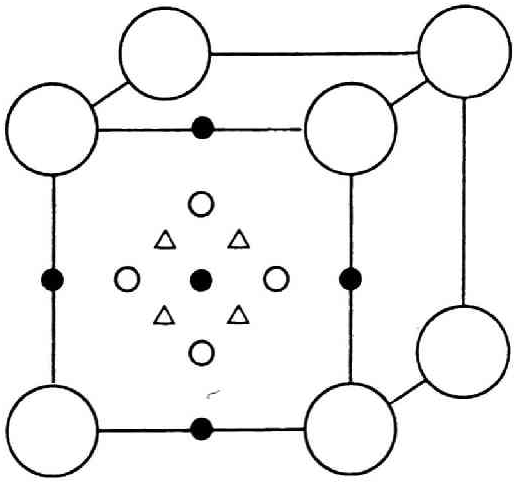

Fig. 1.1

The structure of α-AgI.

● : 6(b) sites, ○ : 12(d) sites, △ : 24(h) sites

large circle : Iodine ion

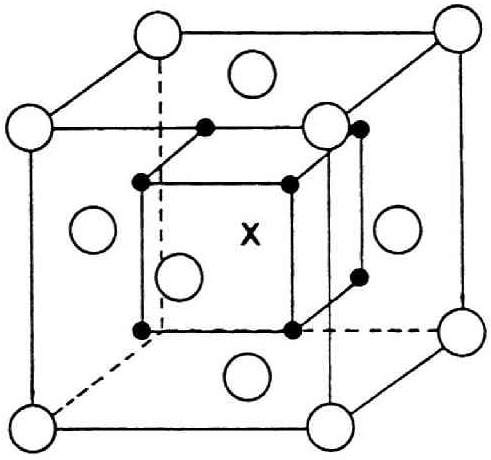

Fig. 1.2

The structure of CaF_2.

● : tetrahedral sites, **X** : octahedral sites

circle : Calcium ion

how to determine the interaction potential. It is well known that in simple liquid such as argon the short range repulsive part of the pair potential plays an important role in structural and dynamical properties and the phase transition of the system. The soft-core system, characterized by the inverse power repulsive potential

$$\varphi(r) = \varepsilon(\frac{\sigma}{r})^n, \tag{1.1}$$

was widely studied as a model of rare gas systems and metallic systems. It was shown that the soft-core system with $n \lesssim 7$ realizes the three-phase behavior of softer metals, that is, a low temperature close-packed phase, an intermediate temperature bcc phase and a high temperature fluid phase.[34] The thermodynamic properties of this "three-phase model" were studied by Hiwatari and Matsuda.[35] The dynamical properties of the soft-core system were studied in detail by Hiwatari *et al.*[36] by the MD method.

In this work we apply the soft-core system to the ionic system. The simple and natural extension of the soft-core system to a charged system may be to assume the pair potential as

$$\varphi_{ij}(r) = \varepsilon(\frac{\sigma_i + \sigma_j}{r})^n + \frac{Z_iZ_j(fe)^2}{r}, \tag{1.2}$$

where σ_i and Z_i are the effective core radius and the valence of ion i, respectively. The ionicity f is also introduced. In what follows the system with the pair potential (1.2) will be called *the ionic soft-core system*. As is described in chapter Ⅱ, the ionic soft-core system has a simple scaling property similar to that of the soft-core system. The equilibrium state is characterized by only a few dimensionless parameters. This makes it easy to understand the interrelation between the physical properties of the system and the characteristics of the interaction potential. The potential (1.2) was first applied to SIC's by Hiwatari and Ueda in their Monte Carlo(MC) studies of α-AgI[37] and CaF_2.[38] Their works were extended by Fukumoto *et al.*[39,40] who performed the MD simulation of α-AgI with the potential (1.2). They examined the relation between the potential parameters and the existence of the α-phase. Using the data of Fukumoto *et al* . Hokazono *et al.*[41] studied the dynamical structure of α-AgI. They examined the correlation between the diffusive motion of Ag^+ ions and the vibration of the I^--sublattice. The present study is based on these works.

The contents of this article are organized as follows.

In chapter Ⅱ we first describe the scaling law of the ionic soft-core system. We give the physical interpretation of the scaling parameters in relation with the scaling law of the soft-core system and that of the OCP. Secondly we present the computational method of the MD simulations.

Chapters Ⅲ, Ⅳ and Ⅴ are devoted to the study of α-AgI. In Chapter Ⅲ we study the interrelation between the superionic conductivity and the interionic potential. The region in scaling parameters σ_{Ag}/σ_{I}, Γ and T^{*}(defined in chapter Ⅱ) within which the superionic state is realized is semiquantitatively determined. The results are interpreted in view of the scaling law. We discuss the characteristic feature of the potential which gives rise to the α-phase. It is found that Pauling's concept of the additivity rule of the ionic radii is necessary for the stability of the I^{-}-sublattice and that the Coulomb force must be appropriately weak for the diffusion of Ag^{+} ions to take place.

In chapter Ⅳ we study the self-diffusion of Ag^{+} by the following three approaches. First we investigate the correlation between diffusing Ag^{+} and a tetrahedron in the I^{-}-sublattice. The characteristics of the driving force of the diffusion is examined. Secondly we analyze the space and time correlation functions. The static structure factor and the self intermediate scattering function are calculated. Finally we have produced a 16mm movie from the MD data in order to see the ionic motion directly. The motion of Ag^{+} ions looks more liquid-like than expected from numerical results so far obtained. Strongly correlated motions of Ag^{+} and I^{-} are also observed.

The collective motion in α-AgI is investigated in

chapter V. The dynamical structure factors and the current correlation functions are calculated. Correlated motions of mobile and immobile ions are investigated by partial dynamical structure factors together with the spectra of the velocity autocorrelation functions. The transverse modes are also examined by both the dynamical structure factors and the transverse current correlation functions. It is clarified that the vibrational motions of Ag^+ and I^- are strongly correlated in the longitudinal acoustic mode at long wavelengths. The motion of Ag^+, however, has no correlation with the longitudinal optic mode of the I^--sublattice for larger wave vectors. Summarizing the results, the mechanism of the diffusion is presented from a dynamical view point.

Chapters Ⅵ and Ⅶ are devoted to the study of CaF_2.

In chapter Ⅵ, after summarizing the experimental and simulational works on superionic fluorites, we study the dependence of the system on the interionic potential. The influence of the potential, especially of the softness of the soft-core repulsion, on the distribution of F^- is examined. Irrespective of the softness of the potential, F^- does not occupy octahedral voids and the diffusion occurs between tetrahedral sites. The diffusion path, however, largely deflects towards octahedral positions when the repulsion becomes harder.

The dynamics of the diffusion of F^- ions is studied in chapter Ⅶ. It has been considered that F^- diffuses by

discrete hops among the tetrahedral sites, which is in contrast with the diffusion in α-AgI. This picture is confirmed in our present data. The local correlation between F^- and a tetrahedron in the fcc lattice is investigated in the same manner as in case of α-AgI. In CaF_2, the correlation between mobile ions is more prominent than in α-AgI. We closely examine the correlated motions of F^- ions. The motions of F^- ions in a sequence of successive jumps are not identical. A new mechanism of the correlated jumps is suggested. We also study the lattice vibrations in CaF_2. The vibrational properties of CaF_2 are quite different from those of α-AgI. Whereas mobile Ag^+ ions oscillate more slowly than the I^--sublattice, mobile F^- ions oscillate with higher frequencies than the Ca^{2+}-sublattice.

In chapter Ⅷ, main results are summarized from the two viewpoints stated above and the difference between α-AgI and CaF_2 is discussed.

CHAPTER II

MODEL SYSTEM AND METHOD OF COMPUTATIONS

2.1 Scaling properties of the ionic soft-core system

In this section, we introduce the scaling law of the ionic soft-core system following Fukumoto *et al.*.[40] If the ionic soft-core system is applied to α-AgI, the Hamiltonian H is scaled as $H = \varepsilon(2\sigma_I/l)^n\tilde{H}$. The scaled Hamiltonian $\tilde{H}$ is given by

$$\tilde{H} = \sum_i \frac{\tilde{P}_i^2}{2m_I'} + \sum_{i>j} \left(\frac{\sigma_i' + \sigma_j'}{\tilde{r}_{ij}}\right)^n + \sum_{i>j} \Gamma \frac{Z_i Z_j}{\tilde{r}_{ij}}, \qquad (2.1)$$

where $l=(V/N)^{1/3}$, $r_i = l\tilde{r}_i$, $P_i=(m_I l/\tau)\tilde{P}_i$, $m_i'=m_i/m_I$ and $\sigma_i'=\sigma_i/2\sigma_I$. m_I is the mass of an iodine ion and the unit of time τ is given by $l(m_I/\varepsilon)^{1/2}(l/2\sigma_I)^{n/2}$. The Hamiltonian $\tilde{H}$ is characterized by the ratio of the ionic core radii σ_{Ag}/σ_I and Γ defined by

$$\Gamma = \frac{(fe)^2}{l} \Big/ \varepsilon\left(\frac{2\sigma_I}{l}\right)^n. \qquad (2.2)$$

Γ represents the ratio of the Coulomb potential to the soft-core potential. The reduced temperature is given by

$$T^* = k_B T \Big/ \varepsilon\left(\frac{2\sigma_I}{l}\right)^n. \qquad (2.3)$$

If n and the mass ratio are kept constant, the equilibrium state of the system is specified by σ_{Ag}/σ_I, Γ and T^*.

The physical interpretation of the scaling parameters is as follows. The thermodynamic state of the soft-core system with the potential (1.1) is characterized by the reduced density ρ^*,[36] which is related with the reduced temperature T_s^* as

$$T_s^* = k_B T \Big/ \varepsilon \left(\frac{\sigma}{l}\right)^n$$

$$= (\rho^*)^{-n/3}. \qquad (2.4)$$

T_s^* gives the ratio of the kinetic energy to the potential energy. Thus T^* in Eq.(2.3) has the same meaning as that of the soft-core system. In the ionic soft-core system the Coulomb potential is added to the soft-core system. This gives rise to an additional parameter Γ, which represents the ratio of the two potentials. Let us compare our scaling law with that of the OCP. In the classical OCP, the thermodynamic state is specified by the plasma parameter defined as

$$\Gamma_P = \frac{(Ze)^2}{ak_B T}, \qquad (2.5)$$

where $a=(3V/4\pi N)$. If we use the Coulomb energy as the unit of energy, $1/\Gamma_P$ gives the reduced temperature instead of Eq.(2.3). Γ_P is related with our scaling parameters as

$$\Gamma_P \propto \frac{\Gamma}{T^*}. \tag{2.6}$$

To sum up, the soft-core system with (1.1) is extended to a two component system, which gives rise to the parameter σ_{Ag}/σ_I, and extended to a Coulomb system, which gives rise to the parameter Γ. In the limit $\Gamma \to 0$, the ionic soft-core system becomes the two component soft-core system and in the limit $\Gamma \to \infty$, it becomes the two component plasma. If the superionic phase is realized by this system, it must be in some region of Γ. This problem is examined in detail in chapter Ⅲ.

2.2 Computational method of MD simulations

The MD simulation is performed for the states at constant energy and constant volume. The system consists of N particles (N=256~500 for α-AgI and N=324~768 for CaF_2) and a periodic boundary condition is imposed. The equation of motion is integrated by Verlet's algorithm.[42] That is, the difference equations

$$\mathbf{v}_i(t) = (\mathbf{r}_i(t+\Delta t) - \mathbf{r}_i(t-\Delta t))/(2\Delta t) \tag{2.7}$$

and

$$\mathbf{r}_i(t+\Delta t) = 2\mathbf{r}_i(t) - \mathbf{r}_i(t-\Delta t) + \mathbf{a}_i(t)(\Delta t)^2 \tag{2.8}$$

are solved numerically, where $\mathbf{v}_i(t)$, $\mathbf{r}_i(t)$ and $\mathbf{a}_i(t)$ are the velocity, position and acceleration of ion i at time t, respectively. Δt is an appropriate time mesh which is chosen as 1/40 ~ 1/50 of τ.

The Coulomb forces are evaluated by the Ewald method. In order to save the CPU time of computations, we have tabulated the electrostatic energy between two particles at grid points on a three dimensional fine grained lattice which span the cell in advance. At each simulation step, the electrostatic force is computed by the interpolation with

use of the tabulated values.[43]

Eqs. (2.7) and (2.8) are integrated in most cases up to 5000~10000Δt. In the analysis of dynamical properties we extend the simulation up to ~400000Δt in order to obtain reliable results of the time correlation functions. In most of our simulations, the total energy is conserved within a fluctuation of 1%.

CHAPTER Ⅲ

SUPERIONIC CONDUCTIVITY AND INTERIONIC POTENTIAL IN α-AgI

3.1 Introduction

Silver iodide undergoes a phase transition from the low temperature β-phase(wurtzite structure) to the superionic α-phase at 420K and melts at 828K. In the α-phase Ag^+ diffuses through the bcc lattice of I^- ions. The distribution of Ag^+ in the α-phase has been investigated by many workers. Strock[2] and Rahlfs[3] proposed a model in which Ag^+ ions are statistically distributed over the 42 positions, that is, 6(b),12(d) and 24(h) sites.(Fig.1.1) The recent neutron diffraction study of Cava *et al.*[31] clearly showed that the distribution of Ag^+ ions takes the maximum value at 12(d) sites. The X-ray and neutron scattering study[44] and EXAFS study[45] support this fact.

A MD simulation of α-AgI was first performed by Schommers,[46] using the Born-Mayer potential for the short range repulsion. Although the α-phase seemed to be realized, he assumed the unphysical harmonic potential between I^- ions so as to stabilize the bcc lattice. Vashishta and Rahman(VR)[47] succeeded to simulate the α-phase by the potential

$$\varphi_{ij}(r) = A_{ij}\left(\frac{\sigma_i+\sigma_j}{r}\right)^n + \frac{q_iq_je^2}{r} - \frac{1}{2}(\alpha_iq_i^2+\alpha_jq_j^2)\frac{e^2}{r^4} - \frac{W_{ij}}{r^6}, \quad (3.1)$$

where α_i denotes the electronic polarizability. The third

term represents the polarization energy and the fourth the dispersion energy. Their results of the distribution of Ag^+ and the diffusion constant are in agreement with experiment.

Although VR's potential seems realistic, it is complicated to understand which term is important for the results. Fukumoto *et al.* showed that the α-phase can be realized by the first two terms of the potential (3.1). This clearly shows that the short range attractive force is rather irrelevant to the existence of the α-phase. They showed that there exists a range of Γ and temperature in which I^- ions form a stable bcc lattice and Ag^+ ions are diffusive. Let us call the region of scaling parameters in which the superionic state is realized the "α-region". Fukumoto *et al.* outlined the α-region on Γ-T^* plane for σ_{Ag}/σ_I=0.286. The value of σ_{Ag}, which was originally used by VR, is about a half of Pauling's value.[48]

In this chapter we further study the interrelation between the superionic conductivity and the interionic potential. It is examined how the α-region on Γ-T^* plane changes with increasing σ_{Ag}/σ_I and to what value of σ_{Ag}/σ_I the α-region appears. Our problem is to find the region of the three parameters Γ, T^* and σ_{Ag}/σ_I which gives rise to the superionic state. In choosing the ionic radii, we pay attention to Pauling's concept of the additivity rule. He assumed the relation $\sigma_+ + \sigma_-$ = (nearest neighbor distance (n.n.d.)) to assign a crystal radius to various ion species

which are assumed to form a rocksalt structure. In α-AgI, Ag^+ ions are disordered. We examine whether the additivity rule is still required or not as a criterion of the stability of the I^--sublattice as in case of ordinary crystals.

3.2 Parameter setting

In order to investigate the problems stated above, we set up the potential parameters ϵ, f, σ_{Ag} and σ_{I} according to the following three cases.

I. The core radii are kept constant and the Γ-dependence of the system is examined by changing ϵ and/or f.

II. Γ is kept constant and the σ_{Ag}/σ_{I}-dependence of the system is examined.

III. Both Γ and σ_{Ag}/σ_{I} are changed under the condition $\sigma_{Ag}+\sigma_{I}$=n.n.d.

Here the n.n.d. is the value when Ag^{+} is located at a tetrahedral site. The values of the parameters are listed in Table 3.1. Following Fukumoto *et al.*, we put n=7 and the lattice constant of the I^{-}-sublattice is a=5.08Å.

The case I is the extension of the cases studied by Fukumoto *et al.*. The values of σ_{Ag} and σ_{I} are the same as those determined by VR from the relations

$$\sigma_{I} + \sigma_{I} = \text{I-I n.n.d.} \quad (4.4\ \text{Å}), \tag{3.2a}$$

$$\sigma_{Ag} + \sigma_{I} = \text{Ag-I n.n.d.} \quad (2.83\ \text{Å}). \tag{3.2b}$$

The cases Ia, Ib and Ic correspond to the cases C, B and A in Fukumoto *et al.*, respectively. They found that the α-phase exists for Ib and Ic, but not for Ia. In the case Ia, although

		Γ	ε(eV)	f	$\sigma_{\lambda\varepsilon}$(A)	σ_1(A)	$\sigma_{\lambda\varepsilon}/\sigma_1$	$\tilde{\sigma}_{\lambda\varepsilon}+\tilde{\sigma}_1$
I	a	0.99	0.177	0.6	0.63	2.2	0.286	3.1
	b	2.06	0.0851	0.6	0.63	2.2	0.286	2.83
	c	2.75	0.177	1.0	0.63	2.2	0.286	2.71
	d	4.02	0.0851	0.84	0.63	2.2	0.286	2.59
II	a	2.06	0.0851	0.6	0.71	2.2	0.323	2.91
	b	2.75	0.177	1.0	0.79	2.2	0.359	2.86
III	a	4.0	0.0851	0.6	0.8	2.0	0.4	2.8
	b	8.38	0.2354	1.0	1.0	1.8	0.556	2.8
	c	19.1	0.2354	1.0	1.2	1.6	0.75	2.8

Table 3.1

Potential parameters used in our simulations.

Ag^+ ions are diffusive, the I^--sublattice is unstable and has a tendency to deform into a more closely packed structure. The case I*b* reproduces the experimentally observed temperature range of the α-phase and the distribution of Ag^+ is in agreement with experimental results. The data at T^*=0.0611 of I*b* are analyzed extensively for the dynamical problems by Hokazono *et al.*. The parameters of II*a* and II*b* are the same as those of I*b* and I*c*, respectively, except that σ_{Ag} is larger.

Here one needs some remarks on the condition $\sigma_{Ag}+\sigma_I$=n.n.d.. If one compares the values of σ_I of arbitrary two cases, ε must be kept constant. According to the scaling law, the characteristics of the scaled system remain unchanged as far as Γ and σ_{Ag}/σ_I are kept constant even if ε and f are changed. Therefore when we refer to the condition $\sigma_{Ag}+\sigma_I$=n.n.d., we reduce ε and f to those of I*b* and re-define σ_I and σ_{Ag} so as to keep Γ and σ_{Ag}/σ_I unchanged. The reduced radii are denoted as $\tilde{\sigma}_I$ and $\tilde{\sigma}_{Ag}$. The values of $\tilde{\sigma}_{Ag}+\tilde{\sigma}_I$ are shown in the last column of Table 3.1. For example, in the case I*a* though σ_{Ag} and σ_I satisfy the condition (3.2), the reduced values are $\tilde{\sigma}_{Ag}$=0.7 and $\tilde{\sigma}_I$=2.4, the sum of which is about 10% larger than the n.n.d.. In the case III both Γ and σ_{Ag}/σ_I are changed so as to keep

$$\tilde{\sigma}_{Ag} + \tilde{\sigma}_I = 2.8. \qquad (3.3)$$

The simulations are performed for 256-ion system. Initially I^- ions are placed to form a bcc lattice and Ag^+ ions are distributed over tetrahedral sites. The equations of motion are integrated in most cases up to $5000\Delta t$ and in some cases up to $10000\Delta t$ to confirm the stability of the I^--sublattice, where Δt is taken as 0.928×10^{-14}sec. In order to investigate the degree of the diffusion and the stability of the I^--sublattice, the following calculations are performed. The self-diffusion constant D_{Ag} is obtained from the slope of the mean square displacement $\langle|r(t+s)-r(s)|^2\rangle$, and scaled value D^* is calculated from the relation $D^* = D_{Ag}\tau/l^2$. The mean square amplitude (MSA) of I^- from the lattice sites is evaluated by the value of $\langle|r(t+s)-r(s)|^2\rangle/2$ at large t.[49] The trajectories of ions drawn by the XY-plotter are also examined to find out any indication of deformation of the I^--sublattice.

	T(K)	T*	D_{Ag} ($10^{-5}cm^2/s$)	D*($x10^{-2}$)	MSA(A^2)
	373	0.0407			0.21
	383	0.0415	0.51	0.21	0.28$_5$
	404	0.0441	1.61	0.65	0.29
Ib	453	0.0494	2.60	1.05	0.36
	501	0.0551	2.76	1.11	0.39
	560	0.0611	3.50	1.41	0.44
	668	0.0729	4.69	1.89	0.58
	763	0.0832	5.71	2.30	0.81**
	949	0.0497			0.24*
	1032	0.0540	3.36	0.94	0.39
Ic	1248	0.0654	4.50	1.26	0.48
	1530	0.0801	6.83	1.91	0.60
	1675	0.0877	7.31	2.04	1.06**
	432	0.0471	0.27	0.11	0.30*
Id	537	0.0586	1.42	0.57	0.53*
	599	0.0654	2.28	0.92	melt
IIa	553	0.0603	2.72	1.10	0.49*
	913	0.0478			0.23
	1095	0.0574	0.26	0.07	0.34
IIb	1187	0.0622	3.48	0.97	0.45
	1425	0.0746	4.54	1.27	0.60
	1516	0.0794	5.09	1.42	0.63
	1712	0.0897	6.24	1.74	0.86**
	363	0.0772	0.16	0.09	0.37*
	364	0.0774	1.17	0.66	0.43
IIIa	373	0.0793	1.91	1.08	0.44
	416	0.0885	2.30	1.30	0.54
	452	0.0961	2.88	1.63	0.81**
	874	0.1402			0.46*
	904	0.1450			0.49*
	908	0.1457	2.41	1.18	0.66
IIIb	910	0.1461	0.17	0.08	0.55*
	939	0.1506	1.14	0.56	0.66
	962	0.1544	2.67	1.31	1.06**
	997	0.1600	3.18	1.55	1.15**
	1188	0.1906	4.18	2.04	melt
	641	0.2346			0.37*
IIIc	755	0.2763	0.02	0.01	0.49*
	806	0.2951	0.71	0.52	0.85**
	850	0.3110	2.49	1.84	melt

Table 3.2

Simulation results. The results of Fukumoto *et al.* are also listed. T is the average temperature and T^* is its reduced value. The simulation of the case Id for T=432K and 599 are performed for N=108. (* : The bcc lattice deforms. ** : The diffusive motions of I^- are observed.)

3.3 Results

In Table 3.2 temperature, diffusion constants and MSA of the simulated states are summarized. From these data and the trajectories of ions we carefully examined whether the I^--sublattice in the simulated individual states is stable or not. The examples of the trajectories of I^- are shown in Fig.3.1. Figure 3.1(a) shows the trajectories of the case Ib at T^*=0.0729. Iodine ions form a stable bcc lattice and Ag^+ diffuses with $D^*=1.89\times10^{-2}$. Figure 3.1(b) shows those of the case I*d* at T^*=0.0586. In this case the I^--lattice is slightly distorted from a regular bcc lattice and an irregularity in the diagonal direction is observed. Such a deformation is not reflected in the MSA(=0.53Å^2). The diffusion constant D^* is 0.57×10^{-2}, being small compared with the case shown in Fig.3.1(a). Hereafter the bcc lattice is called stable when such a deformation is not observed.

Concerning the existence of the superionic state, the cases I*a* ~ Ⅲ*c* are classified into three types. The first type is the case for which there exists the temperature range of the α-phase. The cases I*b*, I*c*, Ⅱ*b*, Ⅲ*a* and Ⅲ*b* belong to this type. In all these cases, D^* is of the order of 10^{-2}. For the second type, although there is a temperature range in which Ag^+ ions are diffusive, the bcc lattice is not stable. This is also a superionic state, but D^* is small compared with that of the first type. The case I*d* and Ⅱ*a* belong to this

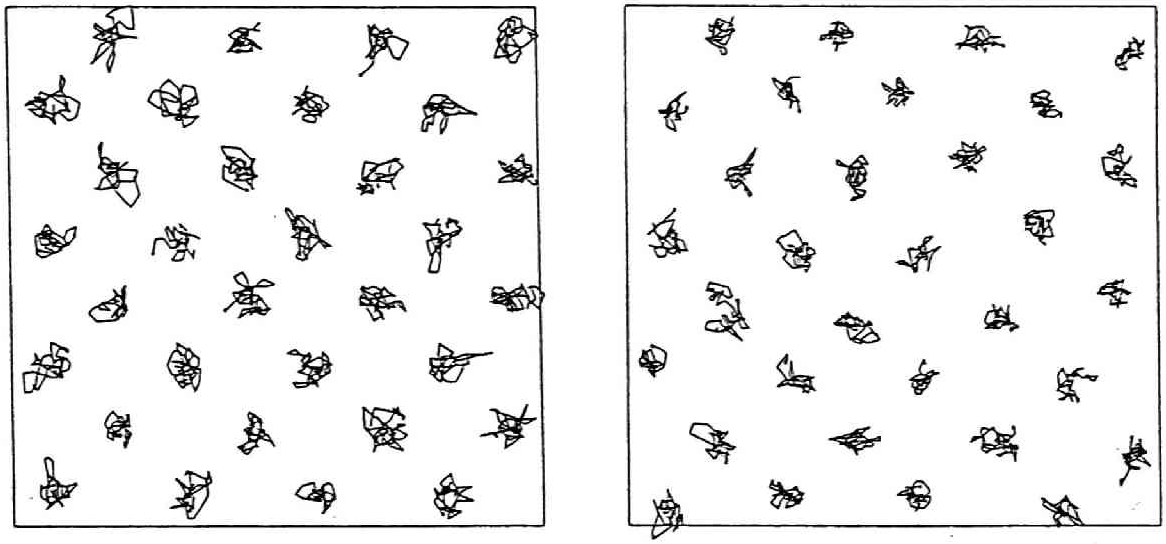

(a) (b)

Fig. 3.1

(a) Trajectories of I^- ions for the stable case Ib (T^*=0.0729). The average positions of ions in two layers for the period of 20Δt are joined by polygonal lines and are projected on to the face of the box. (b) Trajectories of I^- ions for the unstable case Id (T^*=0.0586) plotted in the same way as in (a).

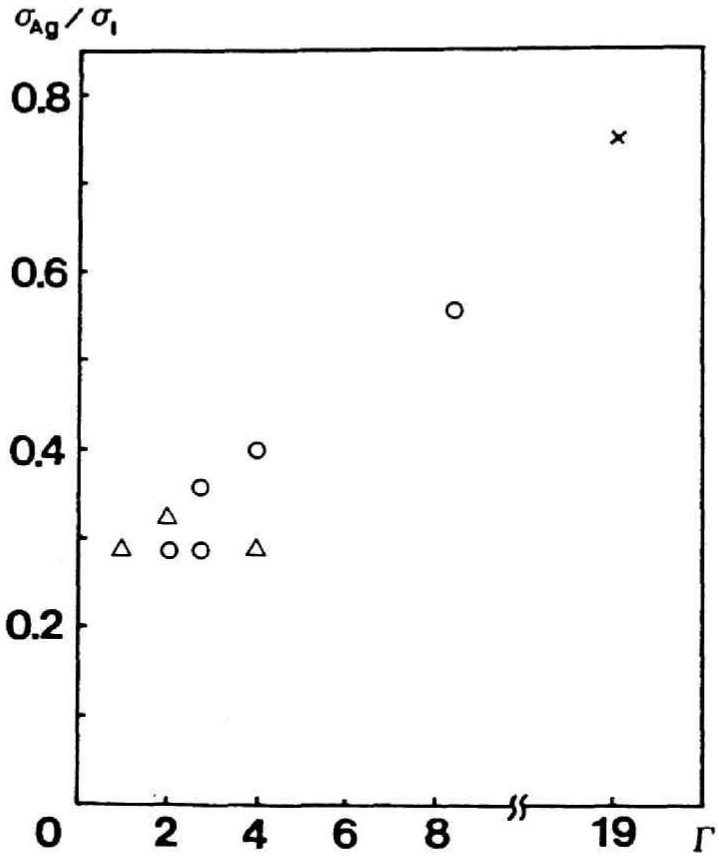

Fig. 3.2

The α-region on the $\Gamma-\sigma_{Ag}/\sigma_I$ plane.

○ : The first type

△ : The second type

X : The third type

type. The case Iα also belongs to this type, for which the deformation of the lattice is more prominent than that of Iδ.[39] The third type is found in the case IIIc for which the superionic state does not exist. Both Ag^+- and I^--lattice melt at the same temperature.

These results are graphically summarized on the Γ-σ_{Ag}/σ_I plane in Fig.3.2, where open circles (○) denote the first type, open triangles (△) the second type and crosses (×) the third type. For σ_{Ag}/σ_I=0.286, $\Gamma \sim 4.0$ seems the upper limit of the α-region. The α-region shifts to large Γ as σ_{Ag}/σ_I increases. Note that with the increase of σ_{Ag}/σ_I from 0.286 to 0.4, the second type(Iδ) becomes the first type(IIIα).

Comparing Fig.3.2 with the last column of Table 3.1, we find that $\tilde{\sigma}_{Ag}+\tilde{\sigma}_I$ is approximately equal to the n.n.d. when the bcc lattice is stable. The deformation of the lattice occurs when $\tilde{\sigma}_{Ag}+\tilde{\sigma}_I$ is larger (Iα,IIα) or smaller (Iδ) than 2.8. This strongly suggests that in the superionic state the condition (3.3) is necessary for the stability of the sublattice. Even if this condition is satisfied, however, the α-phase can not be realized when Γ or σ_{Ag}/σ_I is too large.

Let us examine the temperature dependence of the diffusion constant and the MSA. Figure 3.3 shows $\log D^*$ and the MSA as a function of T^* for the cases of the first type. In Fig.3.3(b) the lines A and B are drawn by eye to distinguish the simulated states according to the degree of

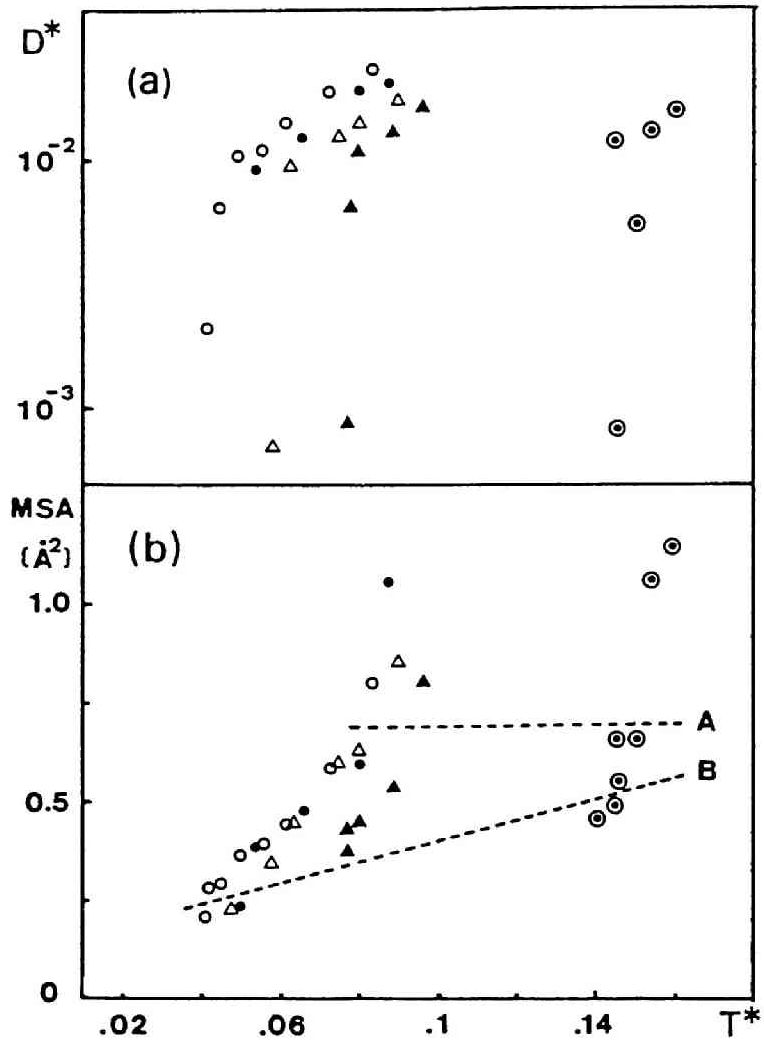

Fig. 3.3

The temperature dependence of (a) the scaled diffusion constants of Ag^+ and (b) the MSA of I^-.

○ : Ib, ● : Ic, △ : Ⅱb,

▲ : Ⅱa, ⊙ : Ⅱb

Ag^+ diffusion and the stability of the I^--sublattice. Points in the region between the two lines correspond to the superionic state. The MSA increases almost linearly with T^* in this region. For Ib, the temperature dependence of the MSA's is in good agreement with experiment, although they are slightly larger than the experimental value evaluated from the Debye-Waller factor B.[31] In this region $\log D^*$ also increases almost linearly with T^* and the slopes are almost the same for each case. The activation energy evaluated from the slope of $\log D_{Ag}$ vs. $1/T$ is about 0.1eV for Ib(T^*=0.0611), which is also in good agreement with experiment.[50]

The states near the line A are considered to be close to the melting temperature T_m of each case. Above this line, not only the amplitude of thermal oscillations is large, but also the diffusive motion of I^- is observed. At low temperature, on the other hand, Ag^+ is not diffusive and oscillates in the vicinity of the tetrahedral sites. The points below the line B correspond to such a state. In some of these states a slight deformation of the I^--sublattice is observed. Such a deformation vanishes when Ag^+ becomes diffusive at high temperature. The temperature at which Ag^+ starts to diffuse will be denoted as T_c. The origin of the deformation of the lattice will be discussed in the next section.

Figure 3.4 shows the α-region on the Γ-T^* plane. For

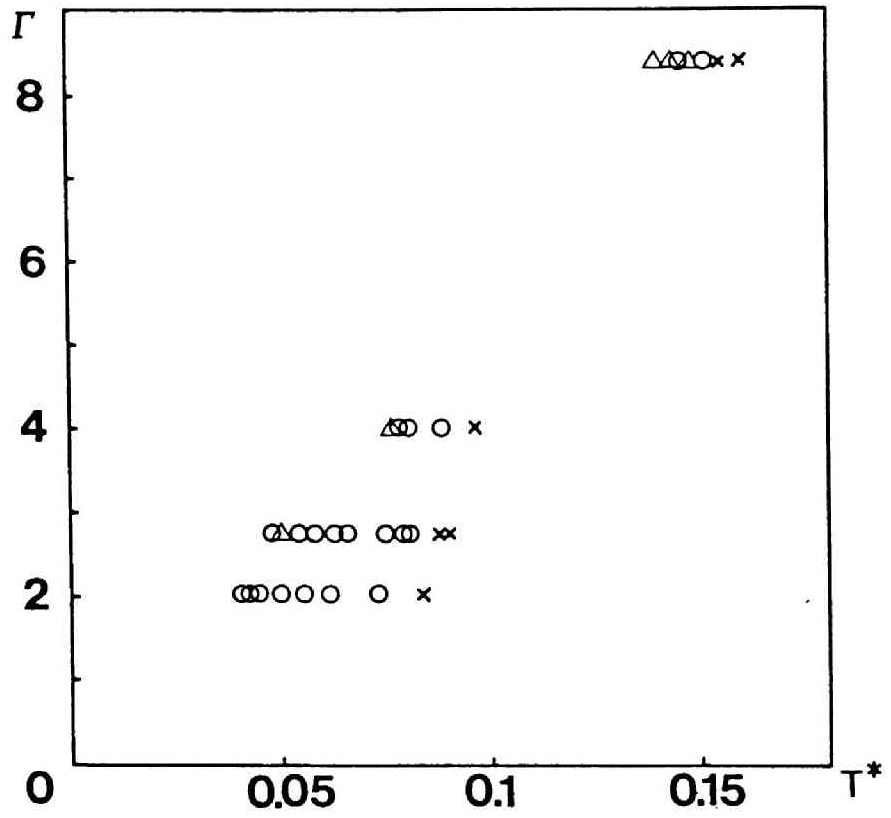

Fig. 3.4

The α-region on the Γ-T^* plane.

The data for Ib, Ic, IIb, IIIa and IIIb are plotted.

○ : bcc lattice is stable.

△ : bcc lattice deforms.

X : near the melting point.

large Γ the α-region shifts to high temperature. When Γ becomes large, T_c approaches T_m and the temperature range of α-region becomes narrower. For IIIb, owing to large Γ and σ_{Ag}/σ_I, the temperature range is very narrow. It is difficult to evaluate accurately the temperature dependence of the physical quantities such as the diffusion constant. This case is considered to be near the upper limit of the α-region.

3.4 Summary and discussion

The α-region in Γ, σ_{Ag}/σ_{I} and T^{*} is semiquantitatively determined. The salient features of our results are summarized as follows.

(1) The condition (3.3), though not strictly as for alkali halide crystals, is necessary for the stability of the I^{-}-sublattice. This implies that the repulsive part of the interaction potential plays an important role for the existence of the α-phase.

(2) Even if the condition (3.3) is satisfied, the α-phase can not be realized if Γ or σ_{Ag}/σ_{I} is too large.

(3) For large Γ, the range of the α-phase shifts to high temperature in the reduced value. The width of the range becomes narrower.

(4) When Ag^{+} is not diffusive at low temperature, there are some cases for which the bcc lattice deforms slightly.

Let us start our discussion with the crystal structure. In α-AgI, the number of tetrahedral sites is six times as large as that of Ag^{+} ions and all sites are energetically equivalent. Thus the crystal is not symmetric if Ag^{+} ions occupy only a part of these sites. This fact is considered as the origin of the deformation of the bcc lattice at low temperature. When Ag^{+} diffuses with a high mobility, every site is occupied with equal probability. As a result the crystal recovers the symmetry and the deformation of the

lattice vanishes. Therefore the diffusion of Ag^+ is important for the stability of the I^--sublattice.

In connection with this fact, there is another reason to be considered for the lattice deformation at low temperature. Fukumoto *et al.* showed that the frequency spectrum of I^- of the case Ib, which is calculated from the Fourier transform of the velocity autocorrelation function, has qualitatively the same feature as that of the Lennard-Jones solid just below the melting temperature. This suggests that the I^--sublattice behaves like a one-component system. Furthermore, the ratios T_m^*/T_c^* of Ib and Ic are ~2.0 and ~1.6, respectively, which agree with the ratio of the melting temperature to the bcc-fcc transition temperature of the soft-core system with n~7 evaluated by Hoover *et al.*[34] Therefore, in addition to the fact mentioned above, the deformation of the I^--sublattice at low temperature is interpreted as the reflection of the bcc-fcc transition of the soft-core system. For Ia, where both $\tilde{\sigma}_{Ag}$ and $\tilde{\sigma}_I$ are large, I^- ions indeed have a tendency to take a more closely-packed configuration even when Ag^- ions are diffusive.[40]

Let us next discuss the α-region in view of the scaling properties of the system. When the constraint (3.3) is imposed, Γ and σ_{Ag}/σ_I are not independent of each other and Γ increases simultaneously with increasing σ_{Ag}/σ_I. Since Γ is the ratio of the Coulomb potential to the soft-core potential, the large Γ corresponds to the state with strong

"Coulomb" force, where "Coulomb" means the relative strength of the Coulomb force in the scaled system. Figure 3.5 shows the pair potential between Ag^+ and I^- scaled by $\varepsilon(2\sigma_I/l)^2$ as a function of the interatomic distance. The position of the minimum of the potential is almost the same for each case, which reflects the condition (3.3). The depth increases with increasing Γ owing to the large "Coulomb" potential. Therefore the diffusion of Ag^+ is suppressed for large σ_{Ag}/σ_I. In other words, an appropriately weak "Coulomb" force is necessary for the superionic phase to appear. That is, $\Gamma \lesssim 8.0$. The shift of the temperature region towards high temperature shown in Fig.3.4 is also attributed to the change in the depth of the potential.

In order to reproduce the observed temperature range of α-AgI from 420K to 828K, Γ must be rather small as the case Ib. One of the parameters which is related with the smallness of Γ is the ionicity f. It is introduced to take the effect of the covalent interaction into account in our rigid ion model. Actually in the case Ib with f=0.6, the temperature range is from ~430K to ~790K. If we set f=1.0 as in the case Ic, the α-region shifts to much higher temperature region. In this sense the weak "Coulomb" is related with the partially covalent interaction between Ag^+ and I^-. The experimental value of f, which was determined from the measurement of the phonon dispersion curves, is 0.56.[16]

The discussions so far given on the existence of the

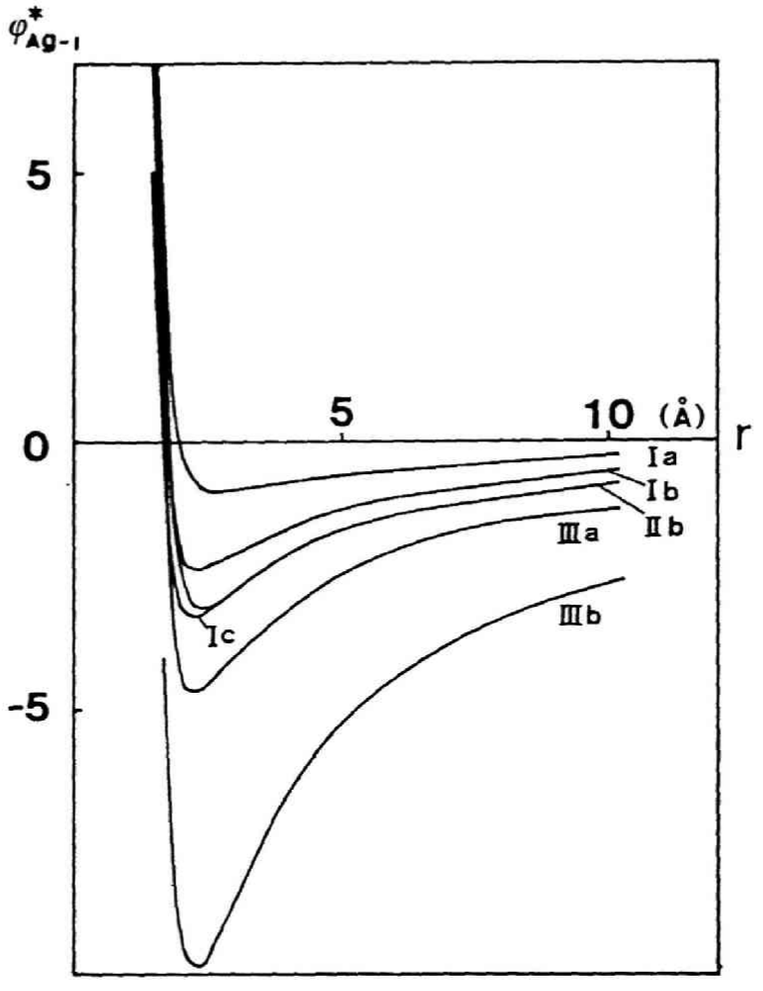

Fig. 3.5

The pair potential between Ag^+ and I^- scaled by $\epsilon(2\sigma_I/l)^n$.

α-region are summarized schematically in Fig.3.6.

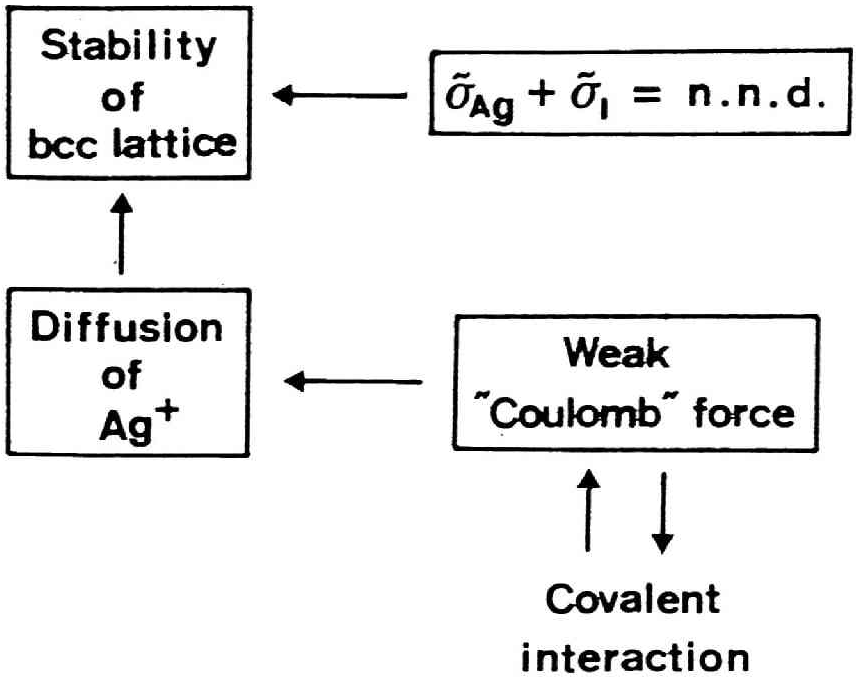

Fig. 3.6

Illustration of the summary of our discussions.

CHAPTER Ⅳ

SELF-DIFFUSION OF Ag^+ IN α-AgI

4.1 Introduction

In this chapter we study the dynamics of the self-diffusion in α-AgI. As is stated in chapter I, Ag^+ ions are distributed over the tetrahedral sites(t-sites) of the bcc lattice. However, the amplitude of thermal vibrations of Ag^+ is quite large and the density distribution extends continuously to the nearest neighbor t-sites.[31] Moreover, the velocity autocorrelation function of Ag^+ has a similar feature to that of a molten salt. These facts suggest that Ag^+ behaves like a liquid enclosed by the cage of the I^- bcc lattice. Hence the 't-site' is not an appropriate concept to indicate the instantaneous positions of Ag^+ ions. For this reason Hokazono *et al.*[41] paid a special attention to a tetrahedron(TH) in the I^- bcc lattice instead of t-sites. The residence time of Ag^+ in a TH was evaluated without any ambiguity. The successive movement of Ag^+ among TH's and the dynamical correlations between Ag^+ and TH's were also examined.

We present the results of the further analysis on the diffusion of Ag^+ among TH's. In order to investigate the driving force of the diffusion we calculate the potential energy experienced by Ag^+ which moves from a TH to its n.n. TH and examine the time variation of the potential barrier along the diffusion path. The contributions of the Coulomb force and the soft-core force to the diffusion are examined

separately. The diffusion of Ag^+ is also examined by calculating the correlation functions. The static structure factor and the self intermediate scattering functions are analyzed. In order to see the correlated motion of ions, we have also produced a 16mm movie from the MD data with use of the computer graphics system. The data used in this chapter are the same as those analyzed by Hokazono *et al.*. The potential parameters are those of the case Ib and the average temperature is 560K. The system consists of 256 ions and the equations of motion are integrated up to $30000\Delta t$ with $\Delta t=0.928\times10^{-14}$sec.

We briefly summarize the results of Hokazono *et al* for convenience of later discussions. In Fig.4.1 we denote the TH made up of I^- ions numbered 1, 2, 3 and 4 as TH(1324). TH(3524) has four nearest neighbor TH's, that is, TH(1324), TH(5724), TH(3526) and TH(3548). Each TH contains one t-site. The mean residence time τ of Ag^+ in a TH is 0.62ps and the distribution of τ extends to about 2ps.(See Fig.3 in Ref.41)

Suppose that Ag^+ moves from TH(1324) to TH(3524) in Fig.4.1. The frequencies of the successive movements from TH(3524) to (1)TH(1324), (2)TH(5724), (3)TH(3526) and (4)TH(3548) are 42, 31, 13.5 and 13.5%, respectively. TH(1324) and TH(5724) share the edge 2-4 with TH(3524), but TH(3526) and TH(3548) share the edge 3-5 with TH(3524), the two edges being perpendicular to each other. Since more than

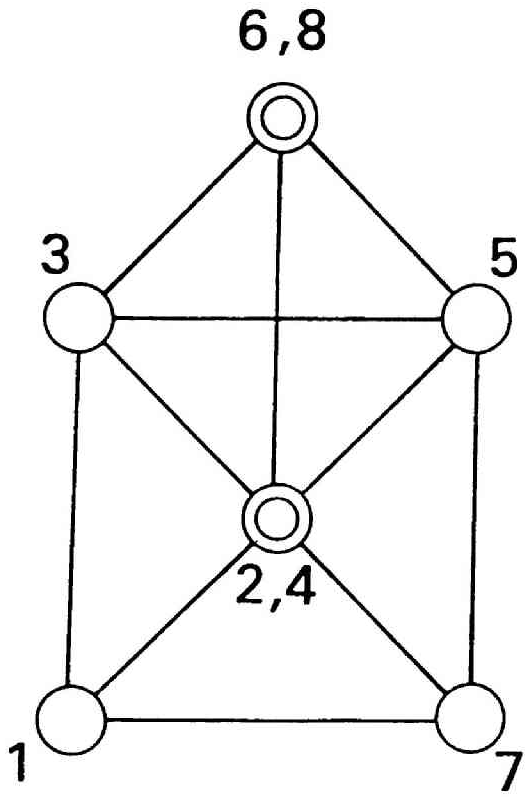

Fig. 4.1

Tetrahedra in the bcc lattice projected on (100)-plane.

70% of the successive movements are those of (1) and (2), the movement of Ag^+ mainly occurs among the four TH's which share the same edge.

To see the dynamical correlation between TH's and the movement of Ag^+, the quantities $P_{kl}=|r_k-r_l|/a$ and $R_{kl}=\frac{1}{2}\frac{d}{dt}(r_k-r_l)^2/av$ are calculated for the pair of I^- ions of k and l when Ag^+ moves from a TH to the adjacent TH. Here a is the lattice constant of the bcc lattice and $v=(3k_BT/m_I)^{1/2}$. They calculated the mean values of these quantities at the instant when Ag^+ reaches the face of a TH. If the movement is assumed to occur from TH(1324) to TH(3524), $\langle P_{24}\rangle$ is 1.061, which shows that the common axis 2-4 is elongated by 6% compared with a. This suggests that the potential barrier at the instant of the movement is lowered. Since $\langle R_{13}\rangle$ is negative(=-0.038) and $\langle R_{35}\rangle$ is positive(=0.036), the distance between I^- of 1 and 3 is decreasing and that between I^- of 3 and 5 increasing. Thus at the instant of the movement TH's deform so as to make the Ag^+ diffusion easier.

4.2 Diffusion of Ag^+ among TH's in the I^--sublattice

In this section we study the driving force of the diffusion. First we pick out Ag^+ trajectories of time interval $300\Delta t$ with an arbitrary initial time(t_0). These trajectories are referred to as 'samples'. They are classified into three cases, A: $d > a$, B: $a > d > a/2$ and C: $a/2 > d$, where d is the distance $|r(t_0+300\Delta t)-r(t_0)|$. Note that the mean square displacement of Ag^+ is about $(a/2)^2$ at $300\Delta t$(=2.78ps).[40] We examined the movements of Ag^+ from one TH to another TH in individual trajectories in the same manner as Hokazono *et al.*. Among 1920 samples, 8270 movements are observed. The contributions of the respective three cases to the diffusion constant D_{Ag} and the frequencies of the successive movements are listed in Table 4.1. Since the movements of the types (3) and (4) are equivalent, they are listed together in the last column as (3)+(4).

In the case A, Ag^+ moves largely, but the contribution to D_{Ag} is small because of rare events. The main contribution to D_{Ag} comes from the case B though the number of samples is only a half of that of the case C. Total frequencies of the successive movements of the type (1), (2) and (3)+(4) are consistent with the results mentioned in section 4.1, but the frequency of (3)+(4) increases with the distance d.

In the following, we use the samples of the case B because they have a large contribution to the diffusion

	Number of samples	Contribution to D_{Ag} ($10^{-5}cm^2/s$)	Number of movements	(1)	(2)	(3)+(4)
A	31	0.54	191	22.5	30.5	47
B	651	2.68	3023	32	30	38
C	1238	0.35	5056	46	33	21
Total	1920	3.56	8270	40	32	28

Table 4.1

Classification of the 'samples' of trajectories and the types of the successive movements. A,B and C are the classes of Ag^+ trajectories defined in the text. The contribution to D_{Ag} is calculated from the slope of the square displacement of the sampled Ag^+ ions. The last three column show the frequencies(%) of the successive movements of the types (1), (2) and (3)+(4).

constant. Among Ag^+ ions moving between TH's we pick out Ag^+ which stays in the initial TH and the final TH for more than $40\Delta t$. The potential energy experienced by Ag^+ along the diffusion path is calculated for the time interval $40\Delta t$, that is, from $-20\Delta t$ to $+20\Delta t$, where the instant of the transition between TH's is set as t=0. Figure 4.2 shows the Coulomb potential and the soft-core potential which Ag^+ would experience if it moves along the path when all the other ions are fixed to the positions at the instant indicated by circles, *i.e.*, $-20\Delta t$, $-10\Delta t$, 0, $10\Delta t$ and $20\Delta t$ (reading from left to right). Here each potential curve in Fig.4.2 is obtained by averaging over the sampled Ag^+ ions. The unit of energy is $e^2/$Å (=14.39eV). The gradient of the curve at the position of circles coincides with the direction of the force acting on Ag^+. Note that the time interval $40\Delta t$(=0.37ps) is slightly shorter than the vibration period of the I^--sublattice evaluated from the spectrum of the velocity autocorrelation function. The mean distance between the initial and final positions of the path is 1.18Å.

It is clearly seen that the soft-core potential barrier becomes lower and lower as Ag^+ moves along the path from a TH to the adjacent TH, which corresponds to the fact described in section 4.1. Especially for the type (1), the soft-core potential is almost "flat" during the movement and effectively no repulsive force acts on Ag^+. On the other hand, for the type (3)+(4) the contribution of the soft-core

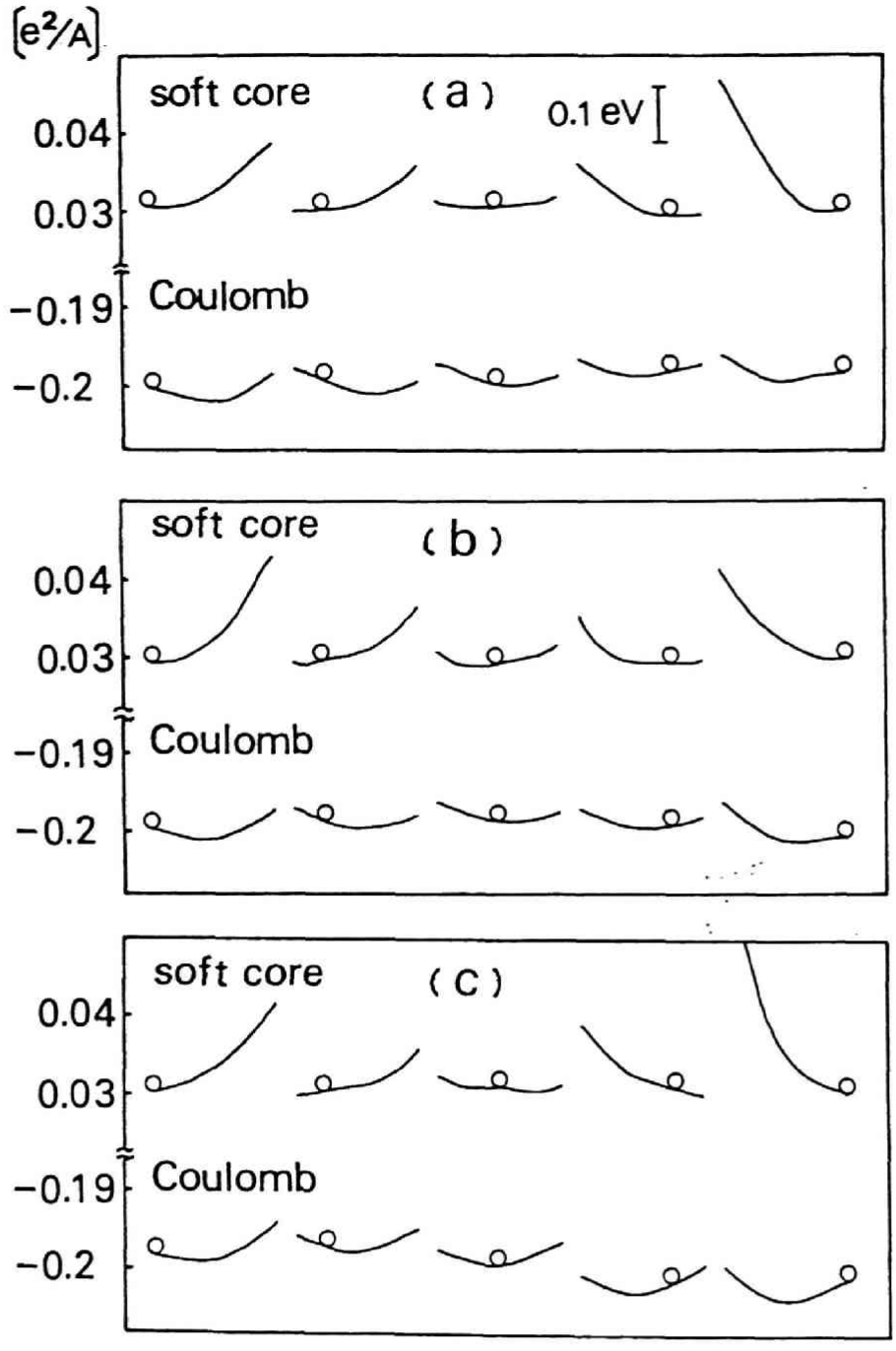

Fig. 4.2

The Coulomb and the soft-core potentials along the diffusion path, (a) for type (1), (b) for type (2) and (c) for type (3)+(4). Circles indicate the times $-20\Delta t$, $-10\Delta t$, 0, $10\Delta t$ and $20\Delta t$ from left. Details of the calculation are stated in the text.

repulsion is prominent especially after the transition. Even at t=20Δt the repulsive force still works in the direction to accelerate the diffusion. Therefore the movement of the type (3)+(4) is influenced by the vibrational motion of I^- ions compared with the cases (1) and (2). This is considered to be due to the difference in the geometrical situation of the TH's involved in the diffusion and the dynamics of I^- ions which form TH's, especially depending on whether they have the common edge or not.

The curves of the Coulomb potential have no significant difference among (1),(2) and (3)+(4). The Coulomb force acts to accelerate Ag^+ in the forward direction for t<0 and in the backward direction for t>0. Thus the main driving force of diffusion is the Coulomb force. The overall feature of the curves of the type (1) is similar to that of (2). As is seen from the curves at 20Δt, the backward force is almost relaxed for these types. Thus the movements of (1) and (2) is expected to occur more smoothly than that of (3)+(4).

4.3 Space and time correlation functions

The static structure factor $S_{\alpha\alpha}(\mathbf{k})$ of ion species α(+ or −) is calculated from the definition

$$S_{\alpha\alpha}(\mathbf{k}) = \frac{1}{N_\alpha}\left\langle \sum_{i,j=1}^{N_\alpha} e^{i\mathbf{k}\cdot(\mathbf{r}_{\alpha i}-\mathbf{r}_{\alpha j})} \right\rangle, \tag{4.1}$$

where N_α is the number of α-ions. The wave vectors are chosen as $(2\pi/a)(\zeta,0,0)$, $(2\pi/a)(\zeta,\zeta,0)$ and $(2\pi/a)(\zeta,\zeta,\zeta)$ with a parameter ζ. Different from the usual structure factor of liquids averaged over the direction of $\mathbf{k}$, $S_{\alpha\alpha}(\mathbf{k})$ is directly related to the intensity of the Bragg scattering. Because of the finite size of the system, the height and the width of peaks depend upon N_α. The results are shown in Fig.4.3.

At (110), (200), (220) and (222) $S_{--}(\mathbf{k})$ becomes large, which corresponds to the Bragg peaks of the bcc structure. This confirms the stability of the I^--sublattice. It should be noted that peaks are also observed in $S_{++}(\mathbf{k})$ at (110) and (200) although they are much lower than those of $S_{--}(\mathbf{k})$. This means that the configuration of Ag^+ ions is predominantly influenced by the structure of the I^- bcc lattice resulting in the Bragg peaks in $S_{++}(\mathbf{k})$ even if Ag^+ behaves like a liquid.

In connection with this result, we investigate the self intermediate scattering function of Ag^+ defined as

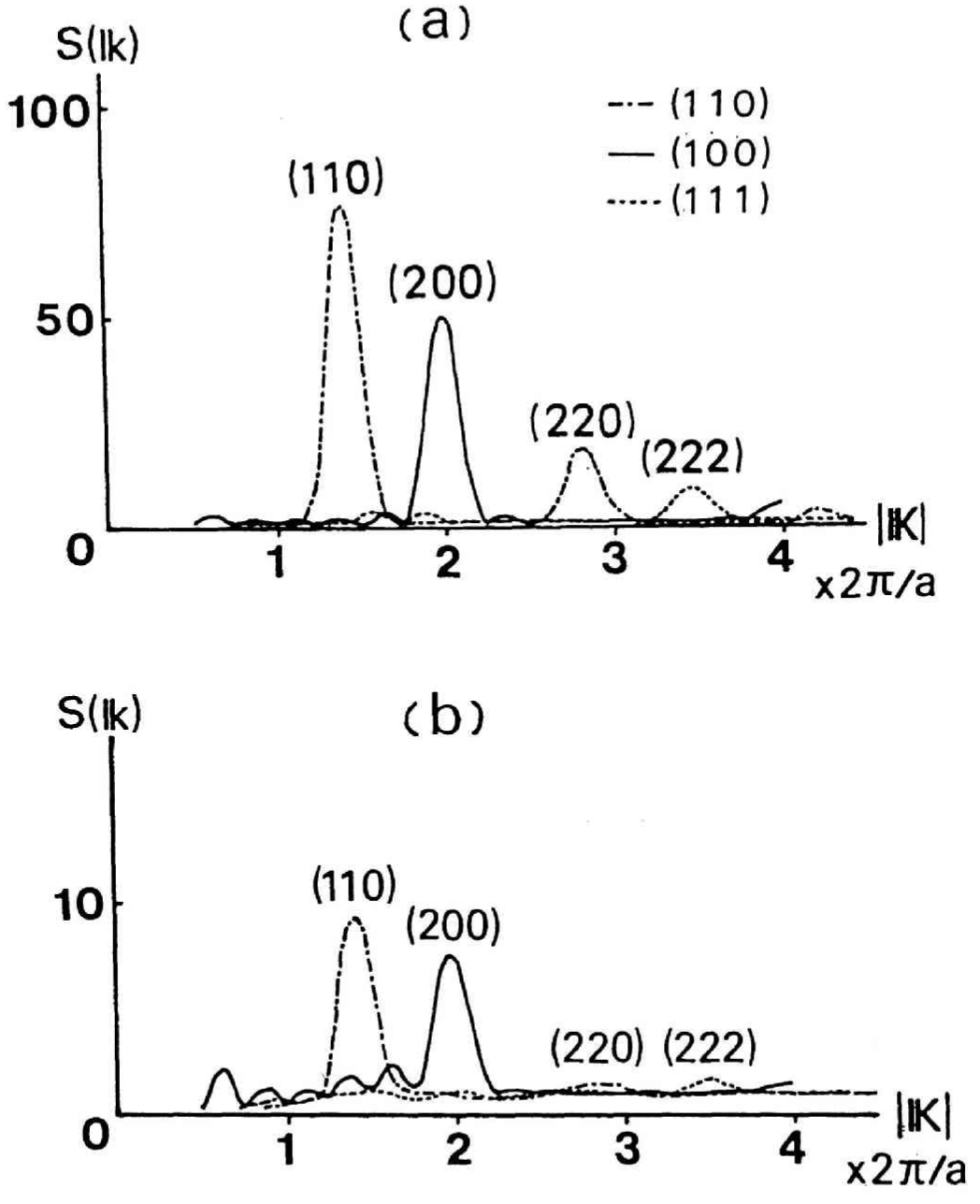

Fig. 4.3

Static structure factor of (a) I^- and (b) Ag^+.

$$F_s(\mathbf{k},t) = \frac{1}{N_+}<\sum_{i=1}^{N_+} e^{i\mathbf{k}(\mathbf{r}_i(t)-\mathbf{r}_i(0))}>. \qquad (4.2)$$

It is calculated for wave vectors in [100] and [110] directions with magnitudes between 0.3Å^{-1} and 6Å^{-1}. The results are shown in Fig.4.4. For sufficiently large or small $\mathbf{k}$, $F_s(\mathbf{k},t)$ is described by only one decay rate, but for the intermediate $\mathbf{k}$, the decay consists of an initial fast decay and a subsequent slow decay. We assume at large t as

$$-\ln F_s(\mathbf{k},t) = \gamma(\mathbf{k})t + c(\mathbf{k}), \qquad (4.3)$$

and evaluate the decay rate $\gamma(\mathbf{k})$ by a least square method. Figure 4.5 shows $\gamma(\mathbf{k})$ for small $\mathbf{k}$ as a function of k^2. In the hydrodynamic limit $F_s(\mathbf{k},t)$ is well described by the isotropic diffusion $F_s(\mathbf{k},t)=\exp(-Dk^2t)$, and the gradient of $\gamma(\mathbf{k})$ is in good agreement with D_{Ag} ($=3.56\text{x}10^{-5}\text{cm}^2/\text{sec}$) calculated from the mean square displacement(the straight line in Fig.4.5).

The Gaussian approximation

$$F_s^G(\mathbf{k},t) = \exp(-\tfrac{1}{6}k^2<|\mathbf{r}(t)-\mathbf{r}(0)|^2>) \qquad (4.4)$$

is also compared with the MD results in Fig.4.4. $F_s^G(\mathbf{k},t)$ agrees with the MD results only for sufficiently small $\mathbf{k}$. For larger $\mathbf{k}$ the agreement becomes poor. The decay rate of

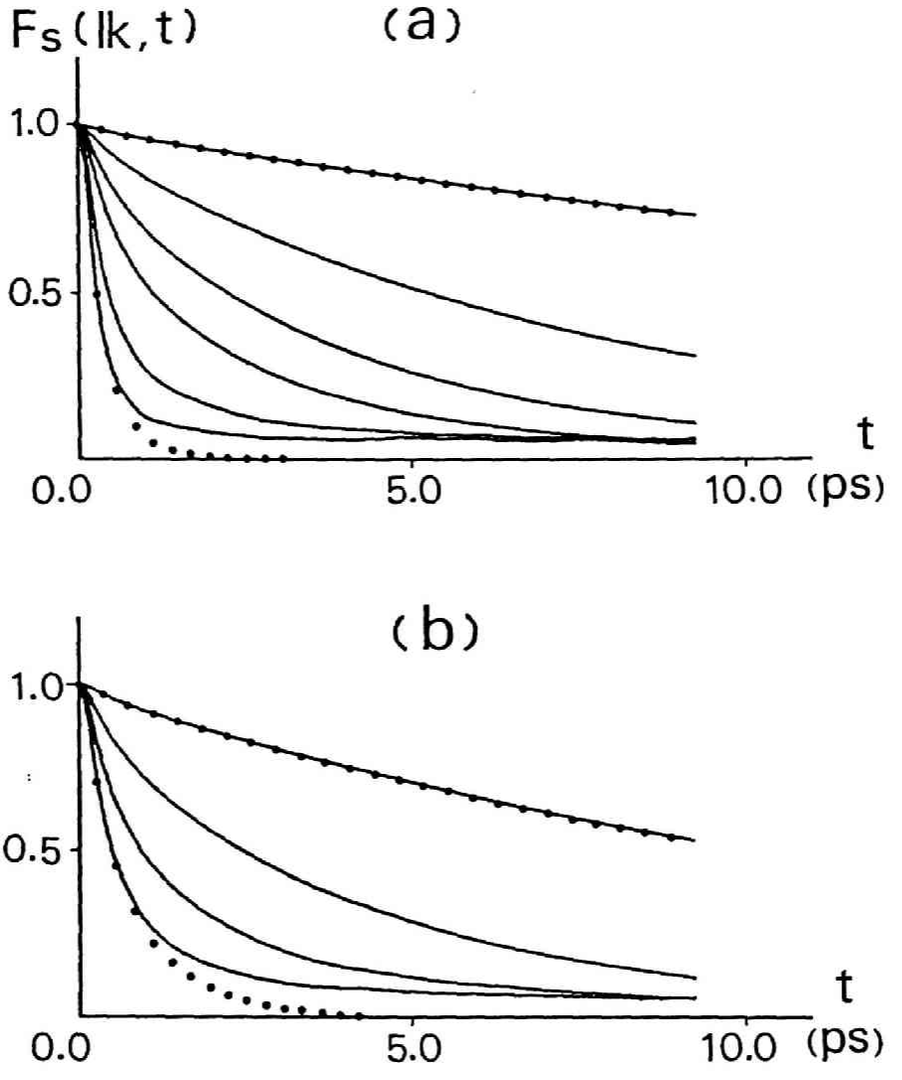

Fig. 4.4

Self intermediate scatterig function of Ag^+. Solid lines show the MD results for (a) $\mathbf{k}=(2\pi/a)(l,0,0)$ with l=0.25, 0.5, 0.75, 1.0, 1.5 and 2.0 from top, and (b) $\mathbf{k}=(2\pi/a)(l,l,0)$ with l=0.25, 0.5, 0.75 and 1.0. The Gaussian approximation $F_s^G(k,t)$ (shown by dots) is compared with MD results for (a) l=0.25 and 2.0, and (b) l=0.25 and 1.0.

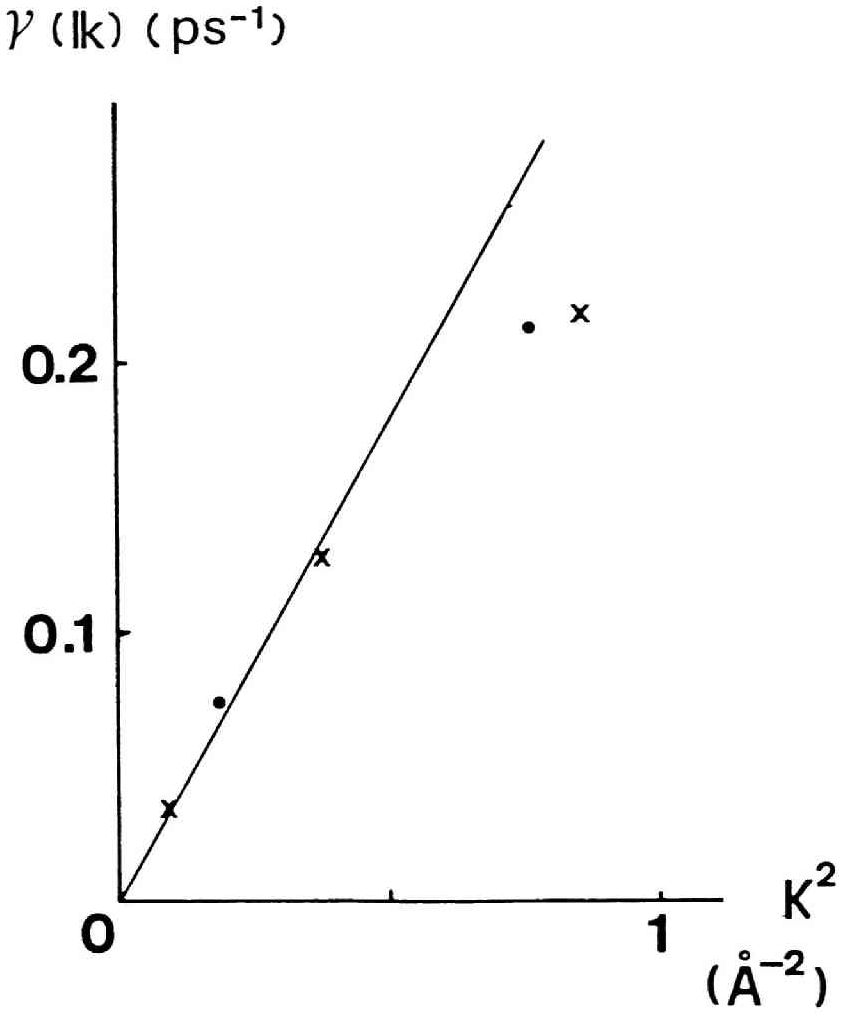

Fig. 4.5

The decay rate $\gamma(\mathbf{k})$ in the hydrodynamic region. The crosses and dots denote the values in the directions [100] and [110], respectively. The solid line shows $D_{Ag}k^2$, where $D_{Ag}=3.56\times10^{-5}cm^2/sec$.

the slowly decaying part of $F_s(\mathbf{k},t)$ is dependent upon the direction of $\mathbf{k}$ and cannot be described by a simple Gaussian function. As is seen in Fig.4.4, for $\mathbf{k}=(2\pi/a)(1,1,0)$ and $(2\pi/a)(2,0,0)$ $F_s(\mathbf{k},t)$ does not vanish at $t\to\infty$, that is, $\gamma(\mathbf{k})\sim 0$. These wave vectors correspond to the positions of peaks of $S_{++}(\mathbf{k})$. This is easily understood by noting that in the limit of $t\to\infty$ $F_s(\mathbf{k},t)$ tends to the same formal expression as the intensity of the elastic Bragg diffraction.[51]

Finally we comment on the inadequacy of the jump diffusion picture of Ag^+. If we apply the Chudley-Elliott jump diffusion model[52] to α-AgI assuming that the diffusion of Ag^+ is described by the instantaneous jumps between t-sites and fit the model to our MD data, the residence time τ at a t-site is estimated as $\tau\sim 2$ps, which is much larger than the mean residence time in a TH.

4.4 Observation of the 16mm movie

With use of the MD data we have produced a 16mm movie of the ionic motion with the aid of a computer-graphics. The snapshots of our film are shown in Fig.4.6. The outermost square shows the real box and in the direction perpendicular to the paper, ions in one fourth of the box are drawn. The dots joined by the straight lines are I^- ions. Ag^+ ions are denoted by open circles. Their trajectories are drawn for time interval 1.86ps. We have observed this film repeatedly to find out the characteristic feature of ionic motions. The results are summarized as follows.

1) Several Ag^+ ions form a momentary configurational order especially in <110> direction. The order appears in any places and in any <110> directions. It lasts for about 0.3~0.5ps and then disappears. We can observe such examples in Fig.4.6(a), that is, Ag^+ ions numbered as (1,2,3,4,5), (6,7,8,9) and (10,11,12,13). Figure 4.6(b) shows the case where no <110> order exists.

2) Most of Ag^+ ions move to and fro in local regions. Occasionally a large motion of Ag^+ is observed such as Ag^+ of 7 and 14 in Fig.4.6(a).

3) The amplitude of the lattice vibration of I^- is large as expected from the large value of the mean square displacement.

4) Ag^+ moves smoothly through the I^--sublattice and exhibit

(a)

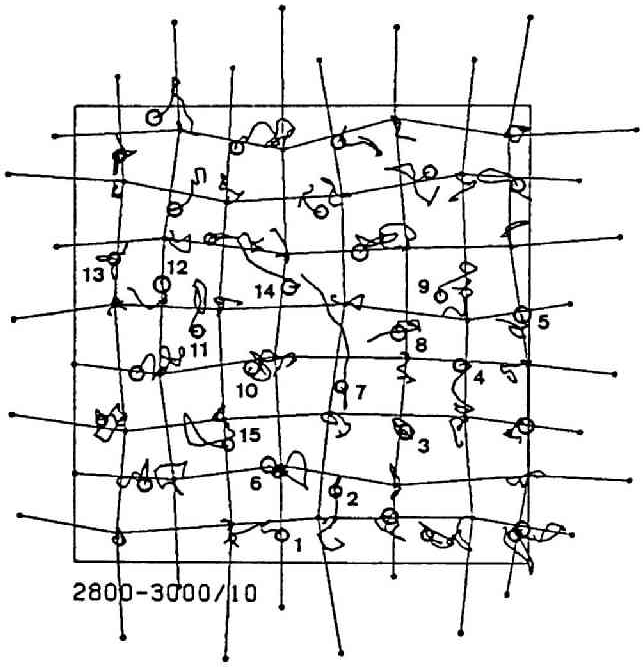

(b)

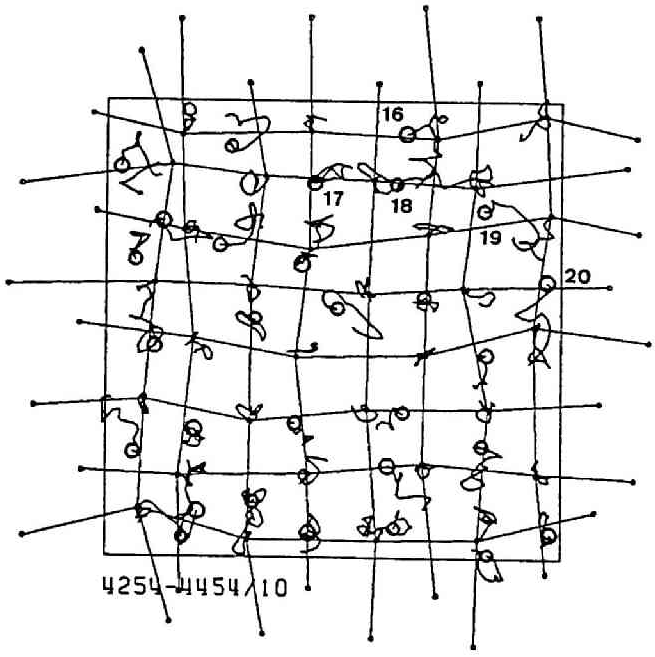

Fig. 4.6

Snapshots of the 16mm movie.

quite a liquid-like behavior. Correlated motions of Ag^+ ions are clearly observed. Several Ag^+ ions move in the same direction at the same time such as Ag^+ ions (16,17,18,19,20) in Fig.4.6(b).

4.5 Summary

We have studied the characteristics of the diffusion in α-AgI by three approaches, that is, the microscopic analysis concerning TH's, correlation functions and the observation of the 16mm movie.

The role of the Coulomb force and the soft-core force for the diffusion process of Ag^+ is clarified. That is, the main driving force of diffusion is the Coulomb force. The soft-core potential barrier becomes lower and lower as Ag^+ moves along the diffusion path, and the potential is almost "flat" when Ag^+ reaches the boundary of TH's. In this sense the repulsive interaction contributes to the movement of Ag^+. However, the mechanism of the diffusion is not such that Ag^+ is "pushed" out of a TH by I^- as expected from the results of $\langle R_{kl} \rangle$ presented in section 4.1.

As is seen from the potential curves for the movements of the types (1) and (2), the diffusion occurs smoothly among the four TH's which share the edge. This suggests that the four TH's form a unit of a local region in which Ag^+ can move rather freely. This is consistent with the results on the frequencies of the successive movements. If this picture is allowed, the movement of the type (3)+(4) occurs when Ag^+ moves from one unit region to another one. In Fig.4.1 such two regions are formed by the TH's which share the edge 2-4 and by those which share the edge 3-5. Note that they have

the common TH formed by the common edges 2-4 and 3-5. In this case, the role of the repulsive force is clearly seen as shown in Fig.4.2(c). Therefore it is considered that a large movement of Ag^+ from one region to another is strongly influenced by the vibrational motion of the I^--sublattice.

From the observation of the 16mm movie the liquid like picture of the motion of Ag^+, which was so far expected from numerical results, is greatly emphasized. As stated in 2) and 4) in section 4.4, the movement of Ag^+ occurs smoothly and is quite different from that of the jump diffusion type. We could directly observe several Ag^+ ions moving in phase and also those moving as if they were dragged by the vibrating I^--sublattice.

CHAPTER V

COLLECTIVE EXCITATIONS AND DIFFUSION MECHANISM IN α-AgI

5.1 Introduction

We studied in chapter Ⅳ the single particle aspect of the diffusion. This chapter deals with the collective motions in α-AgI. As is seen in the 16mm movie, the motion of Ag^+ is strongly coupled with the vibrational motion of the I^--sublattice. We want to investigate such a correlation quantitatively to clarify the mechanism of diffusion from a dynamical point of view.

First we briefly review the MD works on the collective excitations in classical many particle systems. Many workers investigated whether a propagating wave similar to phonons in crystals exists in liquid phases. In simple liquid the Brillouin peak, representing a sound wave propagation, is observed in MD simulations[20,21,24] as well as in the neutron scattering experiments.[53] The existence of a propagating shear wave similar to transverse phonons in crystals was confirmed in fluid phases.[24,54] A MD method is also powerful in studies of the anharmonic effects in crystals. With use of MD results, the validity of the self-consistent phonon theory was examined for rare gas solids[55], ionic solids[29] and metallic solids.[56-58] The collective motions in charged liquids are also studied by the MD method. Hansen *et al.*.[25] showed that the single particle motion in the classical OCP is strongly correlated with the collective plasma oscillation. The dynamical structure factor of the OCP

consists of a sharp peak near the plasma frequency up to the wavelength as small as the nearest neighbor distance and the dispersion relation is typical of the optic mode. In the OCP charge and mass densities are equivalent because of the rigidity of the uniform neutralizing background. In view of our present study, the collective motions in molten salts are more interesting than those in the OCP. It is expected that both the optic and acoustic modes are observed. However, the earlier MD works on molten salts were performed for rather small systems,[26-28] and no trace of the Brillouin peak was observed in these studies. De Leeuw[59] reported that he observed the Brillouin peak as well as the optic-type mode for molten $SrCl_2$ with 324 particles.

In α-AgI collective excitations are expected to reflect both liquid-like and solid-like features, which are correlated with each other. We mainly analyze the dynamical structure factor $S(\mathbf{k},\omega)$ for various wave vectors. The acoustic and optic modes are identified as the peaks of the mass and charge density dynamical structure factors, respectively. We examine how the motions of Ag^+ and I^- contribute to the modes by calculating the partial dynamical structure factors $S_{--}(\mathbf{k},\omega)$ and $S_{--}(\mathbf{k},\omega)$. In order to study the correlation between single particle motions and collective motions, we compare $S(\mathbf{k},\omega)$ with the spectra of the velocity autocorrelation functions(VAF's). It is shown that the vibrational motion of Ag^- is strongly correlated

with the longitudinal acoustic mode of the I^--sublattice for small wave vectors. On the other hand, the I^--sublattice has a high frequency longitudinal optic mode for large wave vectors and the motion of Ag^+ is not correlated with such high frequency motions. In order to analyze the transverse mode, we also calculate the transverse current correlation functions. Summarizing these results and our previous results, we propose the diffusion mechanism in α-AgI in the last section.

5.2 Method of computations

The MD simulations are performed for the 500-ion system for the case Ib. Equations of motion are integrated up to $38000\Delta t$ with $\Delta t=0.929\times10^{-14}$sec. The average temperature and the diffusion constant are 572K and 3.6×10^{-5}cm^2/sec, respectively. We also use the data of the 256-ion system at T=560K analyzed in chapter Ⅳ for comparison.

The Fourier component of the density of ion species α (+ or -) is given by

$$\rho_\alpha(\mathbf{k},t) = \sum_{i=1}^{N_\alpha} e^{i\mathbf{k}\cdot\mathbf{r}_{\alpha i}(t)}, \tag{5.1}$$

where $\mathbf{r}_{\alpha i}(t)$ is the position of α-ion i at time t. Using the definition (5.1), the mass and charge densities are expressed as

$$\rho_M(\mathbf{k},t) = [m_+\rho_+(\mathbf{k},t) + m_-\rho_-(\mathbf{k},t)]/(m_+m_-)^{1/2}, \tag{5.2}$$

$$\begin{aligned}\rho_C(\mathbf{k},t) &= Z_+\rho_+(\mathbf{k},t) + Z_-\rho_-(\mathbf{k},t)\\ &= \rho_+(\mathbf{k},t) - \rho_-(\mathbf{k},t),\end{aligned} \tag{5.3}$$

respectively, where m_α is the mass of α-ion. The partial dynamical structure factor $S_{\alpha\beta}(\mathbf{k},\omega)$ is defined as the spectrum

of the density correlation between α- and β-ions, that is,

$$S_{\alpha\beta}(\mathbf{k},\omega) = \frac{1}{2\pi (N_\alpha N_\beta)^{1/2}} \int_{-\infty}^{\infty} e^{i\omega t} \langle \rho_\alpha(\mathbf{k},t)\, \rho_\beta(-\mathbf{k},0) \rangle dt . \qquad (5.4)$$

The dynamical structure factors representing the mass and charge density correlations are related to $S_{\alpha\beta}(\mathbf{k},\omega)$ by

$$\begin{aligned} S_{MM}(\mathbf{k},\omega) &= \frac{1}{2\pi N} \int_{-\infty}^{\infty} e^{i\omega t} \langle \rho_M(\mathbf{k},t)\, \rho_M(-\mathbf{k},0) \rangle dt \\ &= \frac{1}{N} [m_+^2 N_+ S_{++}(\mathbf{k},\omega) + m_-^2 N_- S_{--}(\mathbf{k},\omega) \\ &\qquad + 2 m_+ m_- (N_+ N_-)^{1/2} S_{+-}(\mathbf{k},\omega)] / m_+ m_- \qquad (5.5) \end{aligned}$$

and

$$\begin{aligned} S_{CC}(\mathbf{k},\omega) &= \frac{1}{2\pi N} \int_{-\infty}^{\infty} e^{i\omega t} \langle \rho_C(\mathbf{k},t)\, \rho_C(-\mathbf{k},0) \rangle dt \\ &= \frac{1}{N} [Z_+^2 N_+ S_{++}(\mathbf{k},\omega) + Z_-^2 N_- S_{--}(\mathbf{k},\omega) \\ &\qquad + 2 Z_+ Z_- (N_+ N_-)^{1/2} S_{+-}(\mathbf{k},\omega)], \qquad (5.6) \end{aligned}$$

respectively.

When a vibrational mode has a long lifetime, the Fourier transform (5.4) becomes difficult because of the slow convergence of the time correlation function. This difficulty can be avoided by evaluating the power spectrum

directly with use of the formula

$$S(\mathbf{k},\omega) = \frac{1}{2\pi N}\int_{-\infty}^{\infty} e^{i\omega t}<\rho(\mathbf{k},t)\rho(-\mathbf{k},0)>dt$$

$$= \frac{1}{2\pi N}\lim_{T\to\infty}\frac{1}{T}\left|\int_0^T e^{i\omega t}\rho(\mathbf{k},t)dt\right|^2. \qquad (5.7)$$

We truncate T at $2^{15}\Delta t$ and the statistical noise is eliminated by convoluting the raw data with a Gaussian filter function.[29,55] The full width at half maximum (FWHM) of the filter is $1.0\mathrm{ps}^{-1}$.

The currents associated with the densities (5.1)-(5.3) are defined as

$$\mathbf{j}_\alpha(\mathbf{k},t) = \sum_{i=1}^{N_\alpha}\mathbf{v}_{\alpha i}(t)e^{i\mathbf{k}\cdot\mathbf{r}_{\alpha i}(t)}, \qquad (5.8)$$

$$\mathbf{j}_M(\mathbf{k},t) = [m_+\mathbf{j}_+(\mathbf{k},t) + m_-\mathbf{j}_-(\mathbf{k},t)]/(m_+m_-)^{1/2}, \qquad (5.9)$$

$$\mathbf{j}_C(\mathbf{k},t) = Z_+\mathbf{j}_+(\mathbf{k},t) + Z_-\mathbf{j}_-(\mathbf{k},t), \qquad (5.10)$$

respectively, where $\mathbf{v}_{\alpha i}(t)$ is the velocity of α-ion i. These currents are divided into two parts, one is parallel to the wave vector (longitudinal current) and the other is perpendicular to it (transverse current). The spectrum of the longitudinal current correlation function is related to

$S(\mathbf{k},\omega)$ by the equation of continuity, that is,

$$C^{L}(\mathbf{k},\omega) = \frac{1}{2\pi N}\int_{-\infty}^{\infty} e^{i\omega t}<\mathbf{k}\cdot\mathbf{j}(\mathbf{k},t)\mathbf{k}\cdot\mathbf{j}(-\mathbf{k},0)>dt$$

$$= \omega^2 S(\mathbf{k},\omega). \qquad (5.11)$$

The partial transverse current correlation function is given by

$$C^{T}_{\alpha\beta}(\mathbf{k},t) = \frac{1}{2(N_\alpha N_\beta)^{1/2}}\mathrm{Tr}<[\mathbf{k}\times\mathbf{j}_\alpha(\mathbf{k},t)][\mathbf{k}\times\mathbf{j}_\beta(-\mathbf{k},0)]>, \qquad (5.12)$$

and similarly the mass and charge current correlation functions are expressed as

$$C^{T}_{ab}(\mathbf{k},t) = \frac{1}{2N}\mathrm{Tr}<[\mathbf{k}\times\mathbf{j}_a(\mathbf{k},t)][\mathbf{k}\times\mathbf{j}_b(-\mathbf{k},0)]>, \qquad (5.13)$$

where a and b stand for M or C. The Fourier spectra of Eqs.(5.12) and (5.13) are calculated by the direct method similar to the formula (5.7). In the following sections, we present our results of $S(\mathbf{k},\omega)$ and $C^{T}(\mathbf{k},\omega)$ in the normalized forms as

$$\overline{S}_{\alpha\beta}(\mathbf{k},\omega) = S_{\alpha\beta}(\mathbf{k},\omega)/S_{\alpha\beta}(\mathbf{k}), \qquad (5.14)$$

$$\overline{C}_{\alpha\beta}^{T}(\mathbf{k},\omega) = C_{\alpha\beta}^{T}(\mathbf{k},\omega)/C_{\alpha\beta}^{T}(\mathbf{k},t=0), \qquad (5.15)$$

where $S_{\alpha\beta}(\mathbf{k})$ is the static structure factor.

Owing to the periodic boundary condition, wave vectors are restricted to discrete values. In the 500-ion system, which consists of 5×5×5 unit cells, $\mathbf{k}$ is restricted to $(2\pi/a)(n_1/5, n_2/5, n_3/5)$, where n_1, n_2 and n_3 denote integers. Similarly the allowed $\mathbf{k}$ becomes $(2\pi/a)(n_1/4, n_2/4, n_3/4)$ for the 256-ion system.

5.3. Results

5.3.1 Longitudinal collective modes

Figure 5.1 shows $\bar{S}_{MM}(\mathbf{k},\omega)$ and $\bar{S}_{CC}(\mathbf{k},\omega)$ in [100] and [110] directions. The peaks of the longitudinal acoustic (LA) mode are observed in $\bar{S}_{MM}(\mathbf{k},\omega)$ for small wave vectors up to $(2\pi/a)(0.6,0,0)$ and $(2\pi/a)(0.4,0.4,0)$. These wave vectors correspond to the wavelength $\lambda \sim 1.7a$. $\bar{S}_{CC}(\mathbf{k},\omega)$ has a peak of the longitudinal optic (LO) mode at a frequency slightly higher than the plasma frequency $\omega_P=12.8ps^{-1}$ and it persists to $\lambda \sim 1.2a$. The dispersion relations of each mode are summarized in Fig.5.2, where the data of the 256-ion system are also shown. The dispersion of the LO mode is negative in [100] direction and almost flat in [110] direction. For large $|\mathbf{k}|$, the broad quasielastic peak grows both in $\bar{S}_{MM}(\mathbf{k},\omega)$ and $\bar{S}_{CC}(\mathbf{k},\omega)$ and the peaks of the LA mode merge into it. $\bar{S}_{MM}(\mathbf{k},\omega)$ and $\bar{S}_{CC}(\mathbf{k},\omega)$ have almost the same structure for $\zeta>1.0$. The broad quasielastic peak is also observed in the neutron scattering experiments.[60]

The partial dynamical structure factors of Ag^+ and I^- are compared in Fig.5.3 for the same wave vectors as in Fig.5.1. For $\zeta=0.2$, $\bar{S}_{++}(\mathbf{k},\omega)$ is almost the same as $\bar{S}_{--}(\mathbf{k},\omega)$ and consists of a sharp peak of the LA mode and a small broad peak of the LO mode. Thus the long-wavelength vibrational properties of Ag^+ are similar to those of the I^--sublattice and are characterized mainly by the low frequency LA mode.

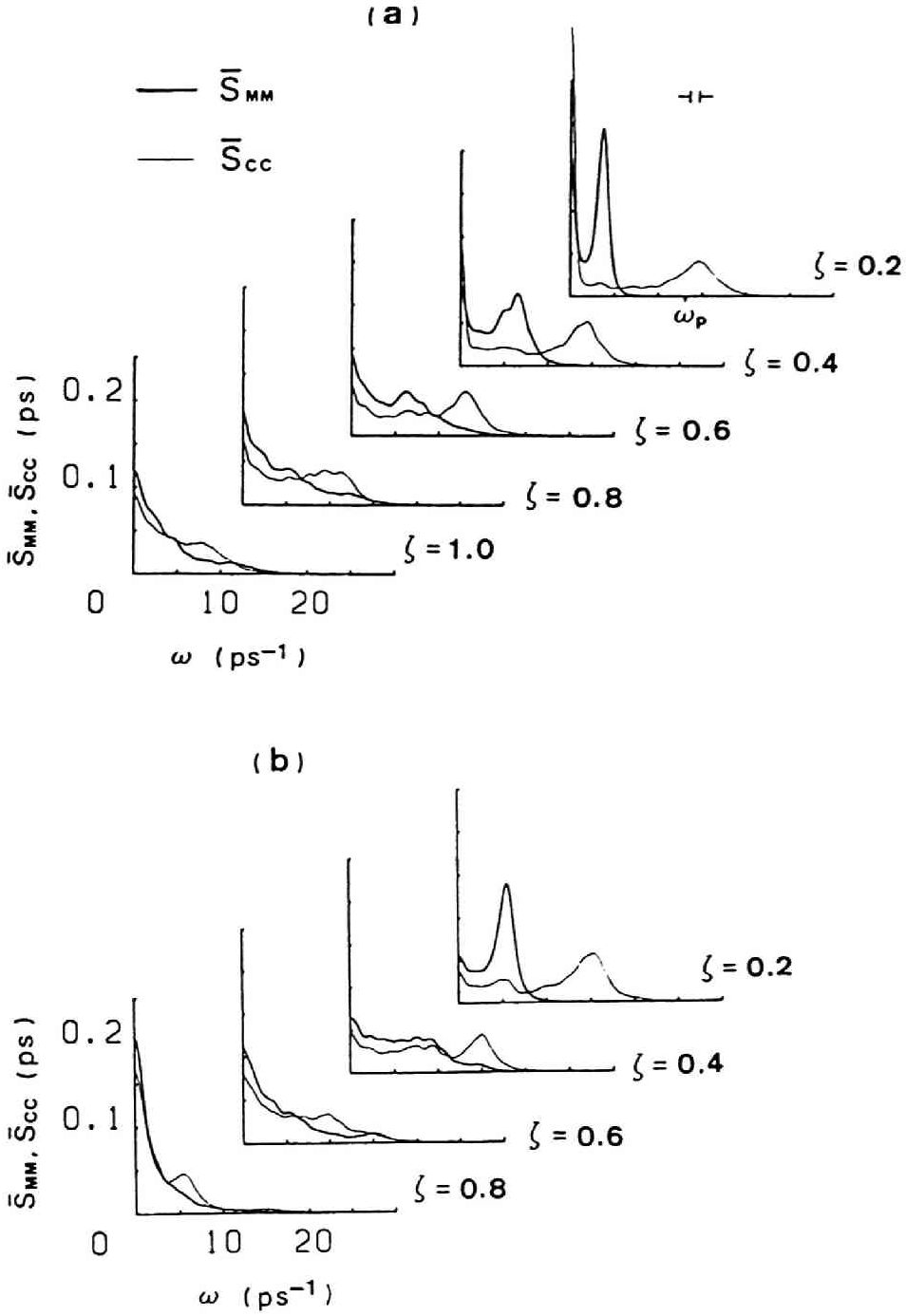

Fig. 5.1

Normalized dynamical structure factors $\bar{S}_{MM}(\mathbf{k},\omega)$ and $\bar{S}_{CC}(\mathbf{k},\omega)$ for (a) $\mathbf{k}=(2\pi/a)(\zeta,0,0)$ and (b) $(2\pi/a)(\zeta,\zeta,0)$. The FWHM of the Gaussian filter function is also shown in (a).

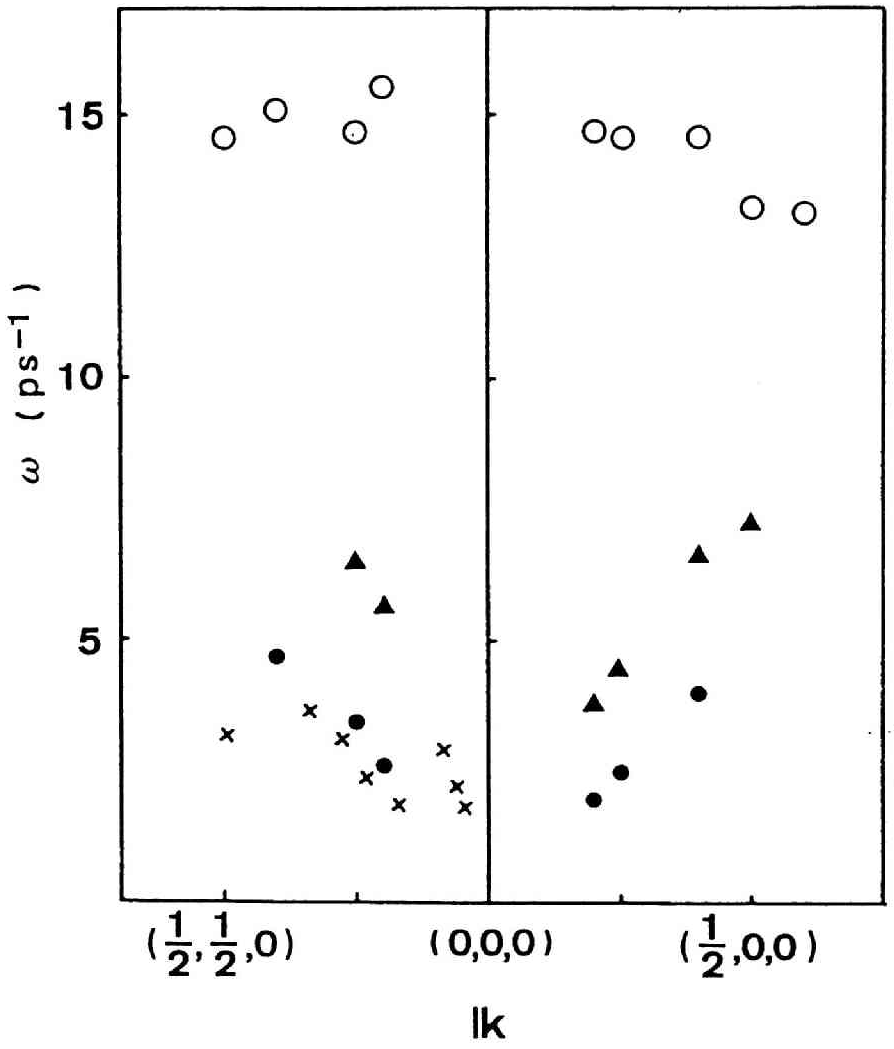

Fig. 5.2

Dispersion relation in [100] and [110] directions ;

○ LO mode ; ▲ LA mode ; ● TA mode.

The results of 256-ion system at T=560K are also shown for ζ=0.25 and 0.5. Crosses are the experimental values of Brüesch *et al.*[62] at T=573K.

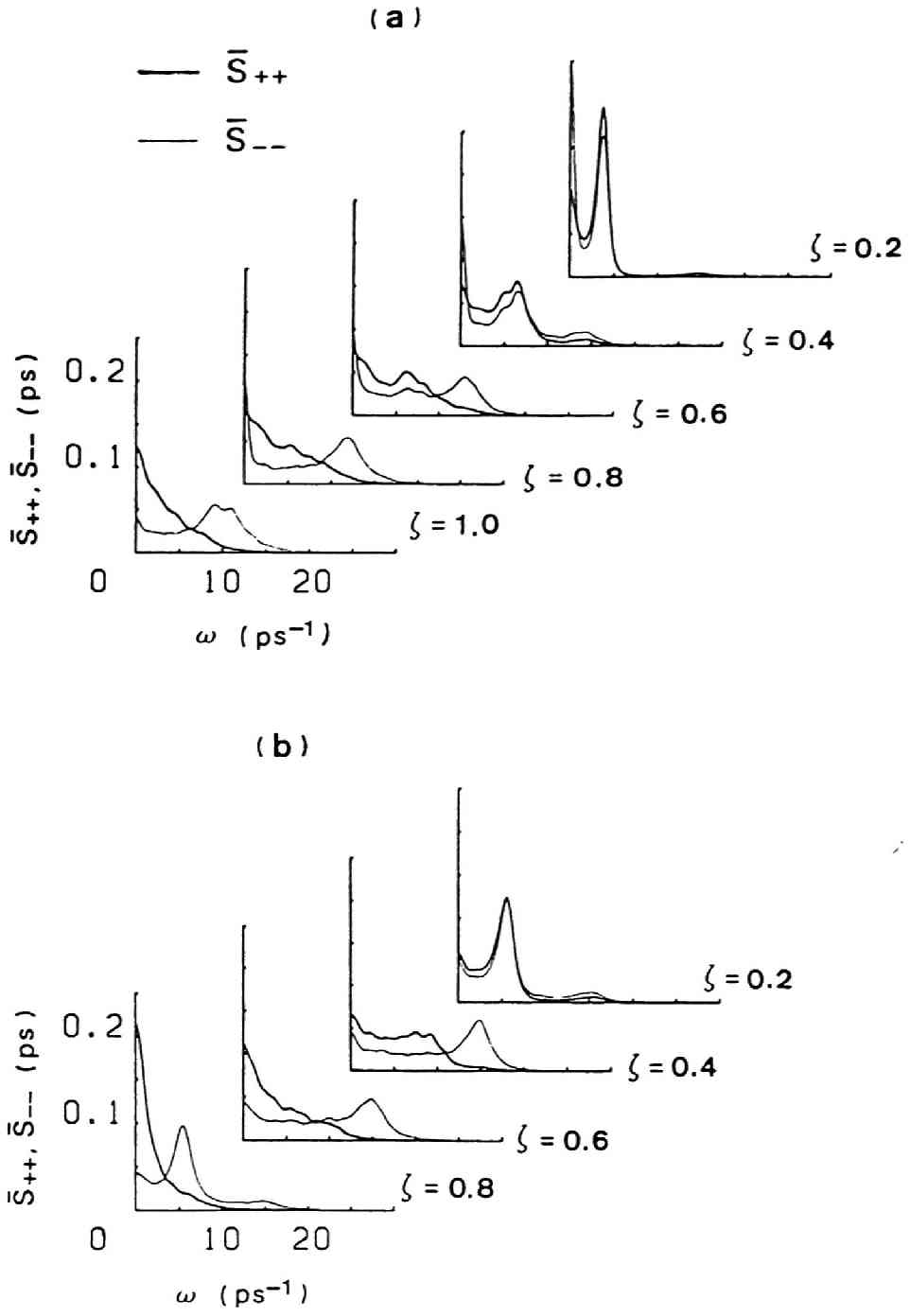

Fig. 5.3

Partial dynamical structure factors $\bar{S}_{++}(\mathbf{k},\omega)$ and $\bar{S}_{--}(\mathbf{k},\omega)$ for (a) $\mathbf{k}=(2\pi/a)(\zeta,0,0)$ and (b) $(2\pi/a)(\zeta,\zeta,0)$.

With increasing |k| the difference between $\bar{S}_{++}(\mathbf{k},\omega)$ and $\bar{S}_{--}(\mathbf{k},\omega)$ becomes evident. While the LO peak is clearly observed in $\bar{S}_{--}(\mathbf{k},\omega)$ even for large wave vectors, $\bar{S}_{++}(\mathbf{k},\omega)$ consists of only a broad quasielastic peak and has no peak as observed in $\bar{S}_{--}(\mathbf{k},\omega)$ at high frequencies. This implies that the motion of Ag^+ has no correlation with the LO mode of the I^--sublattice for large wave vectors.

These results should be compared with the frequency spectrum of the VAF defined as

$$\psi_\alpha(\omega) = \frac{1}{\pi}\int_{-\infty}^{\infty} e^{i\omega t}\frac{<\mathbf{v}_\alpha(t)\cdot\mathbf{v}_\alpha(0)>}{<\mathbf{v}_\alpha(0)\cdot\mathbf{v}_\alpha(0)>}dt. \qquad (5.16)$$

Figure 5.4 shows $\psi_+(\omega)$ and $\psi_-(\omega)$ of the 500-ion system, which agree well with those for the 256-ion system.[40] As is discussed in Ref.41, $\psi_-(\omega)$ has a second peak at $\omega\sim14ps^{-1}$, which is interpreted to arise from the LO mode. However, $\psi_+(\omega)$ consists of only a very broad peak around $\sim5ps^{-1}$ with a small bump near ω_P. Thus the vibrational motion of Ag^+ does not couple with the high frequency LO mode of the I^--sublattice, which directly corresponds to the results on $S(\mathbf{k},\omega)$.

5.3.2 Transverse collective modes

Since the Fourier component of the density contains the coordinate $\mathbf{r}_i(t)$ in the form $\mathbf{k}\cdot\mathbf{r}_i(t)$, only the longitudinal

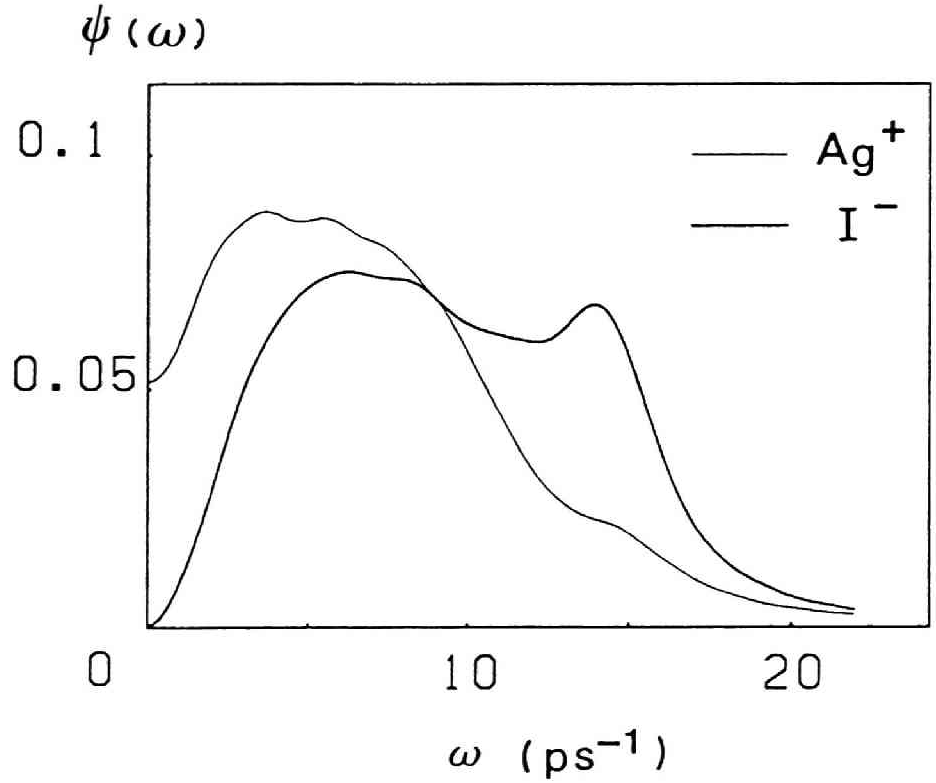

Fig. 5.4

The Fourier spectra of the VAF's of Ag^+ and I^-.

modes are examined by $S(\mathbf{k},\omega)$. In order to investigate the transverse collective modes, we adopt the following two methods which are complementary to each other.

First we calculate $S(\mathbf{k},\omega)$ for $\mathbf{k}=\mathbf{q}+\mathbf{K}$, where $\mathbf{q}$ is the wave vector in the first Brillouin zone and $\mathbf{K}$ is the reciprocal lattice vector perpendicular to $\mathbf{q}$.[61] We take $\mathbf{K}=(2\pi/a)(0,2,0)$ for which both $S_{++}(\mathbf{k})$ and $S_{--}(\mathbf{k})$ have peaks. Examples of our calculations are shown in Fig.5.5 for $\mathbf{k}=(2\pi/a)(0.2,2,0)$ and $(2\pi/a)(0.4,2,0)$. There is a peak of the transverse acoustic (TA) mode both in $\overline{S}_{MM}(\mathbf{k},\omega)$ and $\overline{S}_{--}(\mathbf{k},\omega)$ at the frequency lower than that of the LA mode. For the same wave vectors, $\overline{S}_{++}(\mathbf{k},\omega)$ and $\overline{S}_{CC}(\mathbf{k},\omega)$ consist of a broad quasielastic peak with a bump near the frequency of the TA mode. The dispersion relation of the TA mode is compared with that obtained from the neutron scattering experiment[62] at T=573K in Fig.5.2.

Secondly the transverse motions are examined more quantitatively by calculating the transverse current correlation functions. Figure 5.6 shows the normalized spectra in [100] direction. $\overline{C}^{T}_{MM}(\mathbf{k},\omega)$ has a sharp peak of the TA mode for small $|\mathbf{k}|$'s at the frequency slightly higher than that of the respective $\overline{S}_{MM}(\mathbf{k},\omega)$ in Fig.5.5. In contrast with the TA mode, $\overline{C}^{T}_{CC}(\mathbf{k},\omega)$ consists of a low and broad peak at 5~10ps^{-1} for all wave vectors. Although this is expected to arise from the transverse optic (TO) vibrations, the peak position and the dispersion relation of the mode can not be identified in the present data.

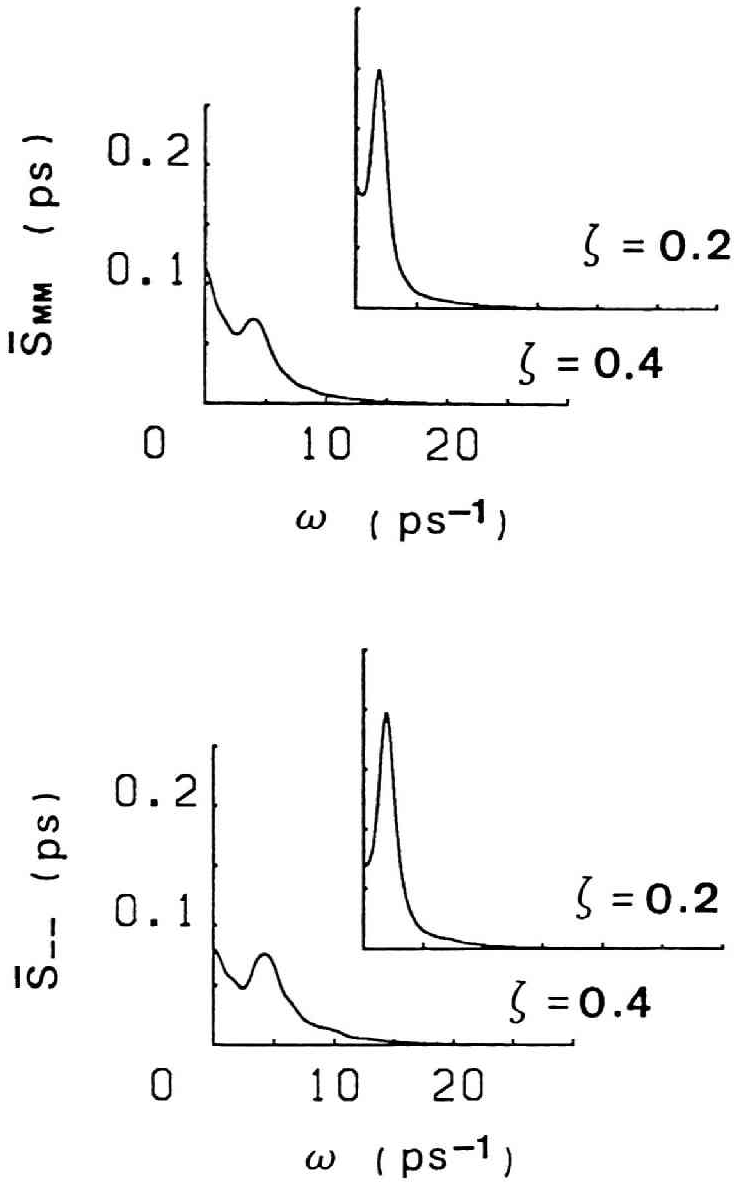

Fig. 5.5

$\bar{S}_{MM}(\mathbf{k},\omega)$ and $\bar{S}_{--}(\mathbf{k},\omega)$ for $\mathbf{k}=(2\pi/a)(\zeta,2,0)$ with $\zeta=0.2$ and 0.4.

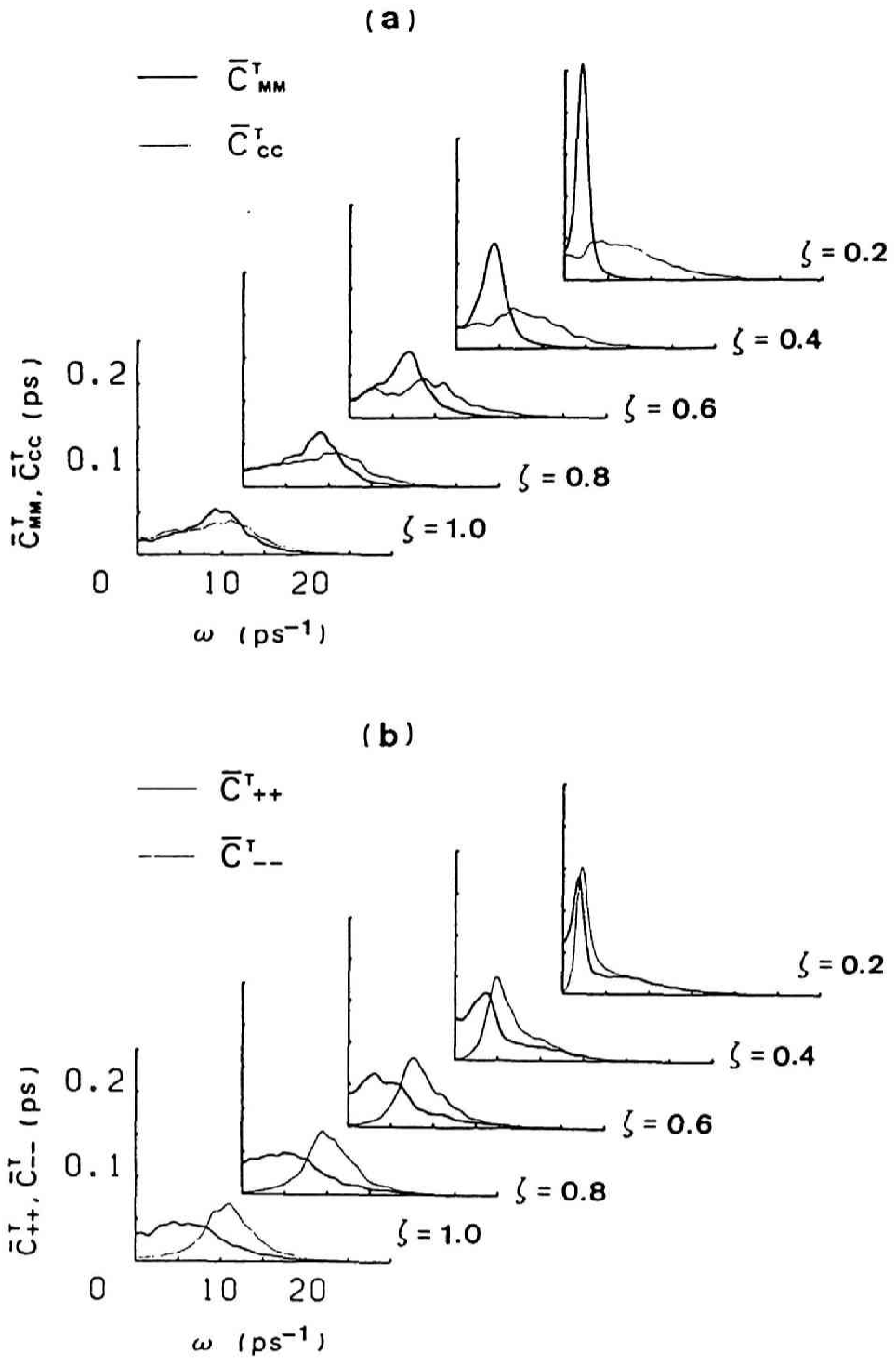

Fig. 5.6

The normalized spectra of the transverse current correlation functions (a) $\bar{C}^T_{MM}(\mathbf{k},\omega)$ and $\bar{C}^T_{cc}(\mathbf{k},\omega)$, and (b) $\bar{C}^T_{++}(\mathbf{k},\omega)$ and $\bar{C}^T_{--}(\mathbf{k},\omega)$ for $\mathbf{k}=(2\pi/a)(\zeta,0,0)$.

In Fig.5.6(b) the peak frequency of $\overline{C}^{I}_{++}(\mathbf{k},\omega)$ is lower than that of $\overline{C}^{I}_{--}(\mathbf{k},\omega)$ and the difference between the two spectra becomes more evident as $|\mathbf{k}|$ increases. The peak in $\overline{C}^{I}_{++}(\mathbf{k},\omega)$ broadens for large $|\mathbf{k}|$, while a clear peak still exists in $\overline{C}^{I}_{--}(\mathbf{k},\omega)$. This suggests that the transverse motions of Ag^{+} and I^{-} do not occur in phase.

5.3.3 Quasielastic peaks

The $\mathbf{k}$-dependence of the half width at half maximum(HWHM) of the quasielastic peaks of $\overline{S}_{++}(\mathbf{k},\omega)$, $\overline{S}_{MM}(\mathbf{k},\omega)$ and $\overline{S}_{CC}(\mathbf{k},\omega)$ is shown in Fig.5.7. At $\mathbf{k}=(2\pi/a)(2,0,0)$ and $(2\pi/a)(1,1,0)$, the width becomes zero within the resolution of the present calculation even for Ag^{+}. These wave vectors corresponds to the positions of peaks of the static structure factors. The narrowing of the peak occurs in the vicinity of these $\mathbf{k}$'s. The widths of the peaks in $\overline{S}_{++}(\mathbf{k},\omega)$, $\overline{S}_{MM}(\mathbf{k},\omega)$ and $\overline{S}_{CC}(\mathbf{k},\omega)$ are almost the same.

In Fig.5.1(a) and 5.3(a), we find a sharp peak at $\omega=0$ in $\overline{S}_{CC}(\mathbf{k},\omega)$ and $\overline{S}_{--}(\mathbf{k},\omega)$ for small $|\mathbf{k}|$, which is much narrower than the quasielastic peaks for large $|\mathbf{k}|$. The interpretation of the narrow peak is suggested by Zeyher in the hydrodynamic theory.[63] Applying Mori's formalism,[64] he studied the collective motions in superionic conductors and showed that there are two non-propagating modes resulting in the narrow and broad central components in $S(\mathbf{k},\omega)$. The broad one, with a constant width and the intensity proportional to k^2, arises

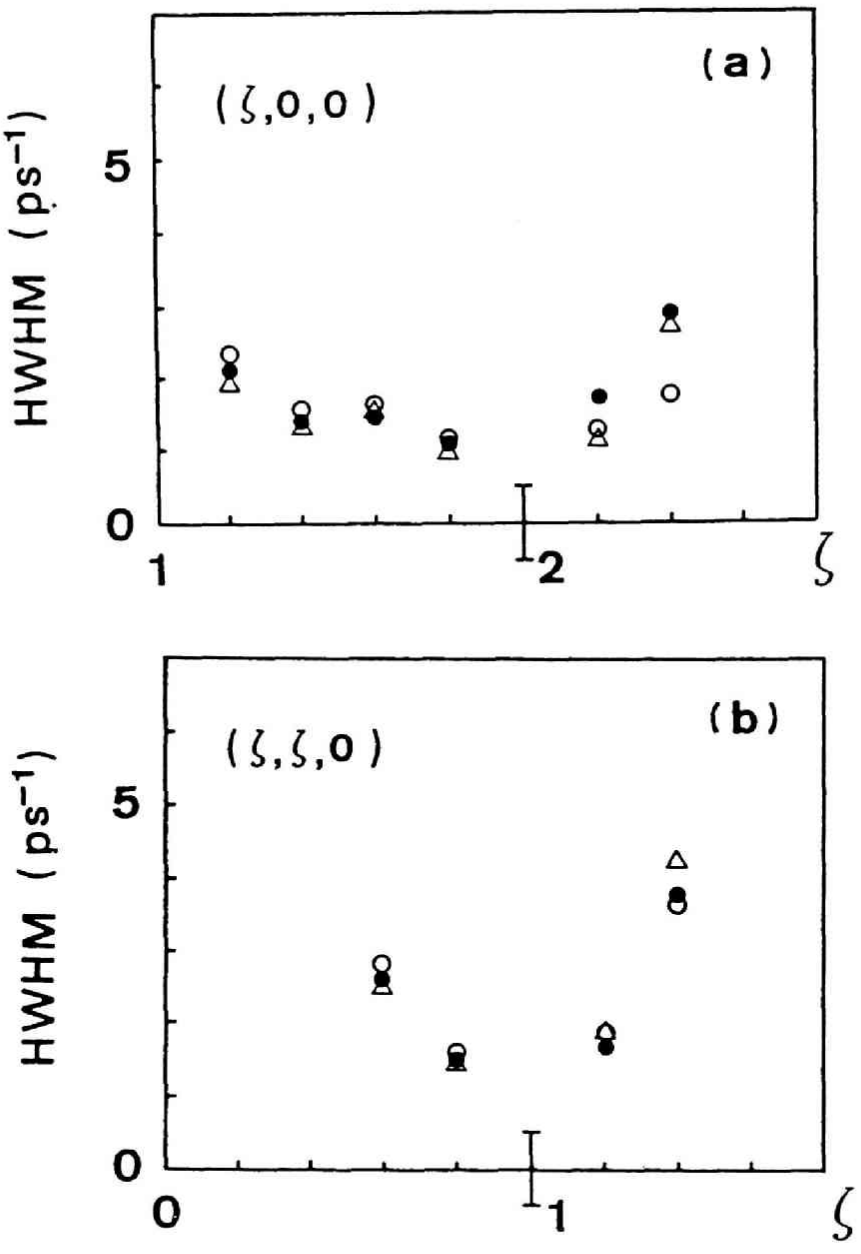

Fig. 5.7

The half width at half maximum of the quasielastic peaks for (a) $k=(2\pi/a)(\zeta,0,0)$ and (b) $(2\pi/a)(\zeta,\zeta,0)$;

● $\bar{S}_{++}(k,\omega)$; ○ $\bar{S}_{CC}(k,\omega)$; △ $\bar{S}_{MM}(k,\omega)$

The bar shows the FWHM of the Gaussian filter function.

from the diffusive motion of mobile ions and the narrow one, with a constant intensity and the width proportional to k^2, is attributed to the energy dissipation. Thus one interpretation of the narrow peak is the effect of the energy dissipation. However, the estimation of the k-dependence of the widths is not possible in the present data because they are less than the FWHM of the window function.

5.4 The mechanism of diffusion

We have studied the characteristic feature of the correlated motions in α-AgI through the dynamical structure factors and the current correlation functions. The main results so far obtained are summarized as follows.

(1) For long wavelengths, the vibrational properties of Ag^+ are similar to those of I^-. The motion of Ag^+ is correlated with the vibrational motion of the I^--sublattice in the low frequency LA mode.

(2) However, the motion of Ag^+ has no correlation with the high frequency LO mode of the I^--sublattice for large $|\mathbf{k}|$. This corresponds to the difference observed in $\psi_+(\omega)$ and $\psi_-(\omega)$.

(3) The frequency of the transverse vibration of I^- is higher than that of Ag^+. This suggests that the transverse motions of Ag^+ and I^- do not occur in phase.

(4) A narrowing of the quasielastic peak of $S_{++}(\mathbf{k},\omega)$ occurs in the vicinity of $\mathbf{k}=(2\pi/a)(2,0,0)$ and $(2\pi/a)(1,1,0)$, which are the positions of peaks in the static structure factors.

On the basis of the results of this and previous chapters, let us discuss the diffusion mechanism in α-AgI. As is mentioned in chapter Ⅳ, the volume of a TH varies rapidly, while Ag^+ contained in it oscillates rather slowly.(See Fig.2 in Ref.41) If the variation of the volume is due to the LO mode, this fact directly corresponds to our

result (2). The diffusive motion of Ag^+ is strongly correlated with the vibrational motion of TH's. Hokazono *et al.* showed that the average volume of TH's which contain Ag^+ is somewhat smaller than that of empty TH's. However, at the instant when Ag^+ moves from a TH to the adjacent TH, the volumes of the two TH's becomes equal. Thus, once Ag^+ moves into a new TH, it shrinks its volume and stores the strain energy. This process results in the local transportation of the strain energy and the lattice vibration of I^- is affected by the diffusion of Ag^+. Moreover, when Ag^+ diffuses, TH's deform so as to make the movement easier. The potential barrier along the diffusion paths becomes lower and lower as Ag^+ moves from a TH to the adjacent TH.

Summarizing these facts, we propose the diffusion mechanism in α-AgI as follows.

[1] Ag^+ oscillates in a TH coupled with the low frequency LA mode at long wavelength.

[2] TH's also oscillate at the high frequency LO mode. When they deform so as to lower the potential barrier, Ag^+ moves out to the adjacent TH.

[3] When Ag^+ diffuses, the relaxation of the local distortion of the I^--sublattice occurs.

[4] Then the strain energy is released to excite the lattice vibration and I^- ions again swing Ag^+.

CHAPTER VI

INTERIONIC POTENTIAL AND DISTRIBUTION OF F^- IN CaF_2

6.1 Introduction

In this and next chapters we study the diffusion in CaF_2. Alkaline earth fluorides, which have a fluorite structure, undergo a phase transition from the low-temperature insulating phase to the high-temperature superionic phase, accompanying a specific heat anomaly. The ionic conductivity gradually increases with temperature and the structure of immobile-ion sublattice is the same in the insulating and superionic phases. The transport properties of this type of superionic conductor were widely studied both theoretically[65,66] and experimentally.[32,33,67,68]

One of the important problems of the ionic conduction in CaF_2 is the distribution of F^- in the superionic phase. The octahedral sites(o-sites), the body centered position and its equivalent positions in the Ca^{2+} fcc lattice, provide the interstitial positions for F^-.(Fig.1.2) It is known that in the low temperature phase an interstitial F^- occupies o-site leaving a vacancy on t-site and that the conduction is due to the interstitial-vacancy pairs. On the other hand, according to the recent neutron scattering experiments[32,33], F^- does not occupy o-sites in the superionic phase and the diffusion occurs among t-sites. Hutchings *et al.*[33] proposed a defect cluster model, which consists of an interstitial F^-, vacancies on t-sites and the distortion in the surrounding lattice. In their model an interstitial F^- is

not situated on *o*-sites, but between *t*-sites slightly shifted towards octahedral positions. Applying this model, they analyzed the data of the diffuse quasielastic neutron scattering experiments.

A lot of MD simulations were also performed for superionic fluorites. Rahman[69] first performed the MD simulation of CaF_2 assuming Kim-Gordon's potential[70] as the short range repulsion. His work was extended by Jacucci and Rahman for dynamical problems.[71] Gillan and his co-workers studied the diffusion in CaF_2[72,73] and $SrCl_2$[74] assuming the Born-Mayer-Huggins potential. They claimed that F^- (or Cl^-) does not occupy *o*-sites and that the diffusion can be analyzed in terms of jumps between *t*-sites. Hiwatari and Ueda[38] applied the ionic soft-core system to CaF_2 in their Monte Carlo (MC) study. In contrast with the results of Gillan *et al.*, it seemed that a large amount of F^- occupy *o*-sites in the superionic phase.

In this chapter we reexamine the distribution of F^- ions in CaF_2. We apply the potential (1.2) and investigate the influence of the interionic potential. We first adopt the same potential parameters as those of Hiwatari and Ueda and modify them appropriately. We study how the occupancy of *o*-sites and the diffusion paths are influenced by the softness of the soft-core repulsion.

6.2 Parameter setting and scaling properties

The Hamiltonian of the system can be scaled in the same way as in α-AgI. We take the soft-core energy between immobile ions as the unit of energy in order that the comparison with α-AgI becomes easier. The Hamiltonian is characterized by the exponent n , the ratio of radii and

$$\Gamma = \frac{4(fe)^2}{l} \Big/ \varepsilon\left(\frac{2\sigma_{Ca}}{l}\right)^n. \tag{6.1}$$

The factor 4 appeared in the right hand side of (6.1) arises from the valence Z_+=+2 of calcium ions. In the case of α-AgI, the dependence of the system on Γ and the ratio of radii was examined, while n is kept constant. In this chapter the dependence on n is also examined.

The values of parameters used in our simulations are listed in Table 6.1. In each case Γ is much larger than that of α-AgI, which reflects a large Coulomb interaction between calcium ions. The parameters of A are those used by Hiwatari and Ueda. The value of ε was fitted to Kim-Gordon's potential[70] between Ca^{2+} and F^- at the nearest neighbor distance(n.n.d). The core radii are chosen so as to satisfy the relation $\sigma_{Ca}+\sigma_F$=n.n.d.. In B we reduce n to 9, retaining other parameters unchanged. The pressure of the system is negative for this case. The parameters of C are chosen so

	n	ϵ(eV)	f	σ_{Ca}(A)	σ_F(A)	Γ
A	12	0.154	1.0	1.28	1.28	157.04
B	9	0.154	1.0	1.28	1.28	153.96
C	7	0.280	1.0	1.28	1.28	83.56

Table 6.1

Potential parameters and the scaling parameters.

that ionic conduction occurs at about 1400K with a positive pressure. The pair potentials φ_{+-} of each case are illustrated in Fig.6.1, together with Kim-Gordon's potential. The potential of C fits well with that of Kim and Gordon except for the repulsive part at a short distance. Following Hiwatari and Ueda, we take the lattice constant a of Ca^{2+} fcc lattice as 5.9Å, which was first adopted in Rahman's work.[69] Although this is slightly larger than the experimental value, we use this value throughout our calculation.

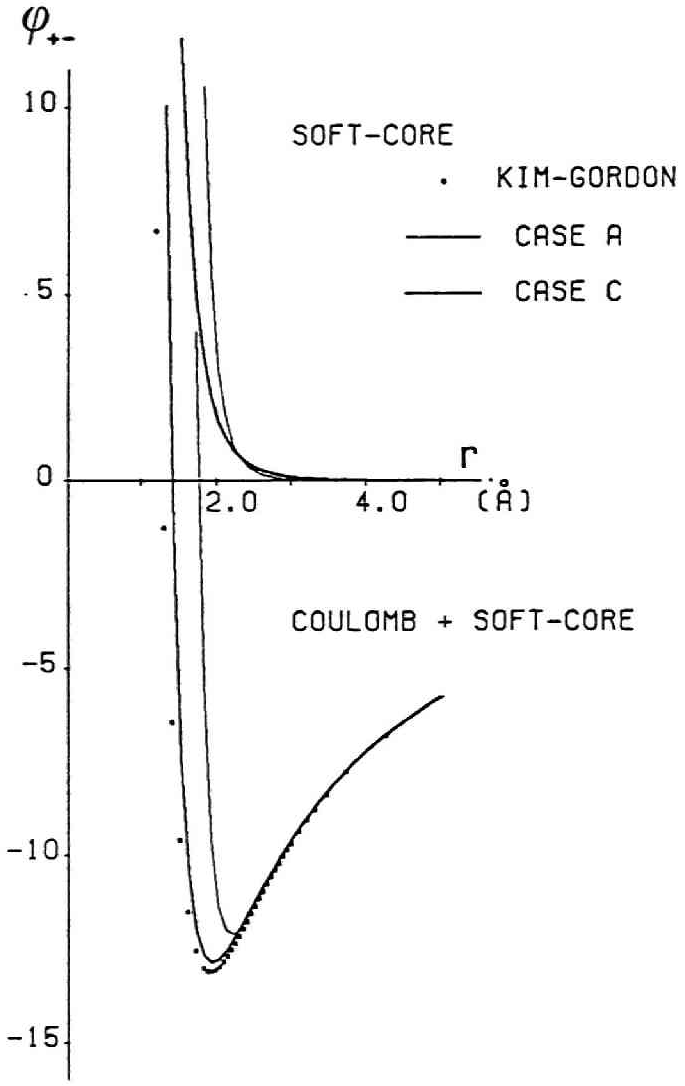

Fig. 6.1

Pair potentials between Ca^{2+} and F^- for A and C, together with Kim-Gordon's potential. The unit of energy is $e^2/Å$.

6.3 results

The MD simulations are performed for the 324-ion system. Initially each ion is placed on the regular sites of the fluorite structure. The average temperature, the compressibility factor, the diffusion constant of F^- and the MSA of Ca^{2+} at each run are summarized in Table 6.2, together with the time mesh Δt. The stability of the Ca^{2+}- and F^--sublattice is examined by studying the trajectories and the radial distribution functions. It is found that in all runs listed in Table 6.2 the Ca^{2+} fcc lattice is stable.

The MD results of A agree with the MC results of Hiwatari and Ueda. The transition to the superionic phase occurs at about 2400K and the melting temperature is higher than 3500K. Note that the experimental values of the transition temperature and the melting temperature are 1423K and 1691K, respectively.[9] In B the transition temperature becomes ~1400K. However, the pressure becomes negative even at the highest temperature. This is the same feature as that of Rahman's work.[69] He showed that the pressure becomes negative even at density $\rho=2.8 g/cm^3$, which corresponds to $a=5.7 Å$.[75] Positive pressure is obtained for C. The temperature dependence of the diffusion constant for C is in agreement with that of Rahman's work performed for $\rho=2.8 g/cm^3$. The melting temperature for the three cases are higher than the experimental value. This may be partly

	T(K)	T^*	PV/NKT	D_F ($10^{-5}cm^2/s$)	D^* (10^{-2})	MSA(A^2)	Δt ($10^{-15}s$)
A	2013	1.219	0.26			0.12	1.95
	2386	1.445	1.58	2.89	1.92	0.18	1.95*
	3020	1.829	2.36	7.74	5.13	0.29	1.95*
B	1027	0.610	-5.89			0.30	2.34
	1620	0.962	-2.09	2.03	1.33	0.34	1.95*
	2055	1.220	-0.54	5.80	3.81	0.47	2.34*
C	1014	0.327	1.48			0.18	2.34
	1210	0.390	1.99			0.20	2.34
	1681	0.542	2.80	2.00	0.97	0.28	2.34*
	2059	0.663	3.09	6.19	2.99	0.35	2.34

Table 6.2

Simulation results. T^* and D^* are the reduced values of average temperature T and diffusion constant D_F, respectively. The compressibility factor and the MSA of Ca^{2+} are also listed. Δt is the time mesh of the integration.
* : The equations of motion are integrated up to $10000\Delta t$, and others $5000\Delta t$.

because the density of the system is kept constant in all temperatures.

The relation between the exponent n and T^* in the superionic phase is illustrated in Fig.6.2. Γ becomes larger as n increases and the temperature range of the superionic phase shifts to larger T^*. Note that the melting point of a soft-core system shifts to higher temperature when n becomes larger.[76] Thus our result is interpreted as the characteristics of the soft-core system.

In all our simulations the ratio σ_F/σ_{Ca} is taken to be unity. If we adopt a larger σ_F/σ_{Ca}, for example, σ_F=1.36Å and σ_{Ca}=1.18Å, the distortion of the F^--sublattice is observed in the low temperature phase. The radial distribution function of the distorted F^--sublattice is similar to that of a fcc lattice. This suggests that the simple cubic structure of F^- is unstable for large σ_F and F^- ions have a tendency to form a more close-packed structure. This is also the case with α-AgI for the case Iα.

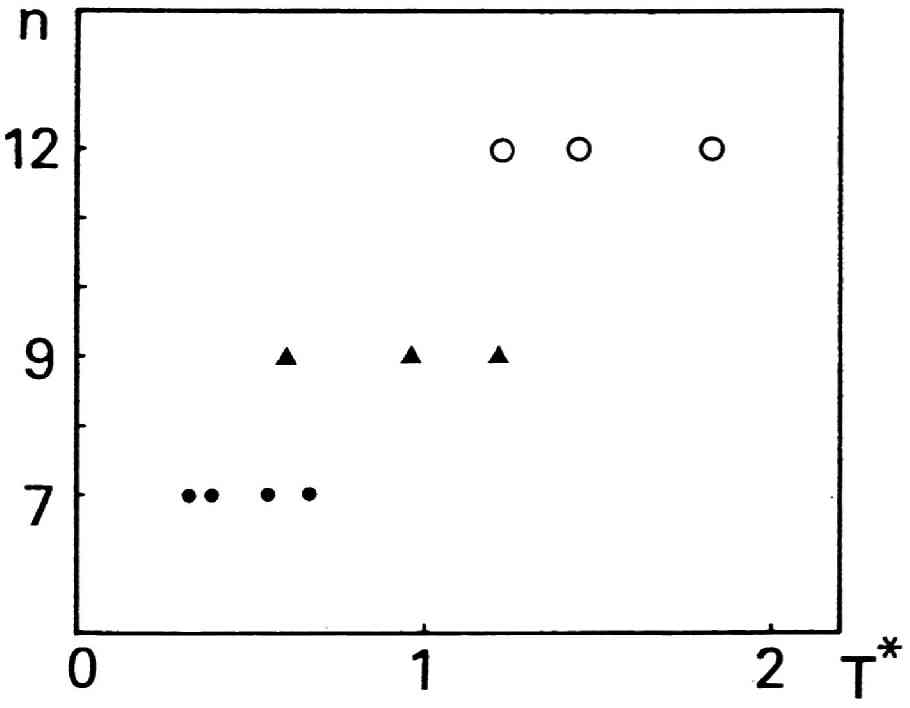

Fig. 6.2

Superionic phase in n–T^* plane for A(○), B(▲) and C(●).

6.4 Influence of the potential on the distribution of F^-

Let us compare the data of A at T=2386K and C at T=1681K. The diffusion constants of these cases are close to that of the data analyzed by Jacucci and Rahman.[71] The trajectories of F^- are compared in Fig.6.3. It is observed in both cases that F^- ions form a simple cubic structure and move among well defined sites, which is in contrast with α-AgI. However, some difference in the diffusion paths is observed between the two cases. Although F^- seems to hop between t-sites in <100> direction in C, the trajectories which pass through o-sites are observed in A. In Fig.6.3(a) a small amount of F^- ions seem to occupy o-sites and the density of F^- ions in the midst of the nearest neighbor t-sites is very low.

In order to examine the distribution of F^- more quantitatively, we have extracted the jump events between sites by counting at every time step the number of F^- inside the spheres with an appropriate radius centered at t- and o-sites. The positions of sites are determined by referring to the time-averaged positions of Ca^{2+} ions. The fractional numbers of F^- ions which occupy t- or o-sites are shown as a function of R, the radius of sphere, in Fig.6.4. The fraction of the octahedral location for A is slightly larger than that for C. In both cases, however, the fraction of the tetrahedral location is much larger than that of the octahedral location. The observed jump events in specified

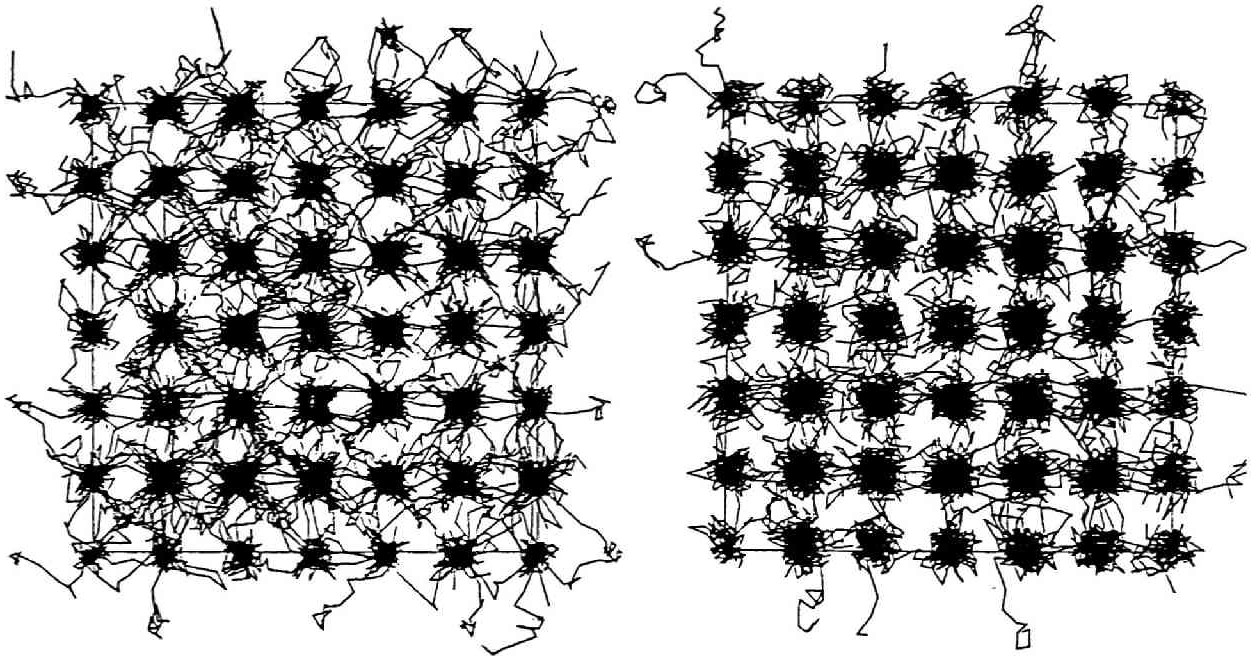

(a) (b)

Fig. 6.3

Trajectories of 216 F^- ions for (a) case A and (b) case C, projected onto a face of the box. The average positions of ions for a period of $504t$ are joined by polygonal lines.

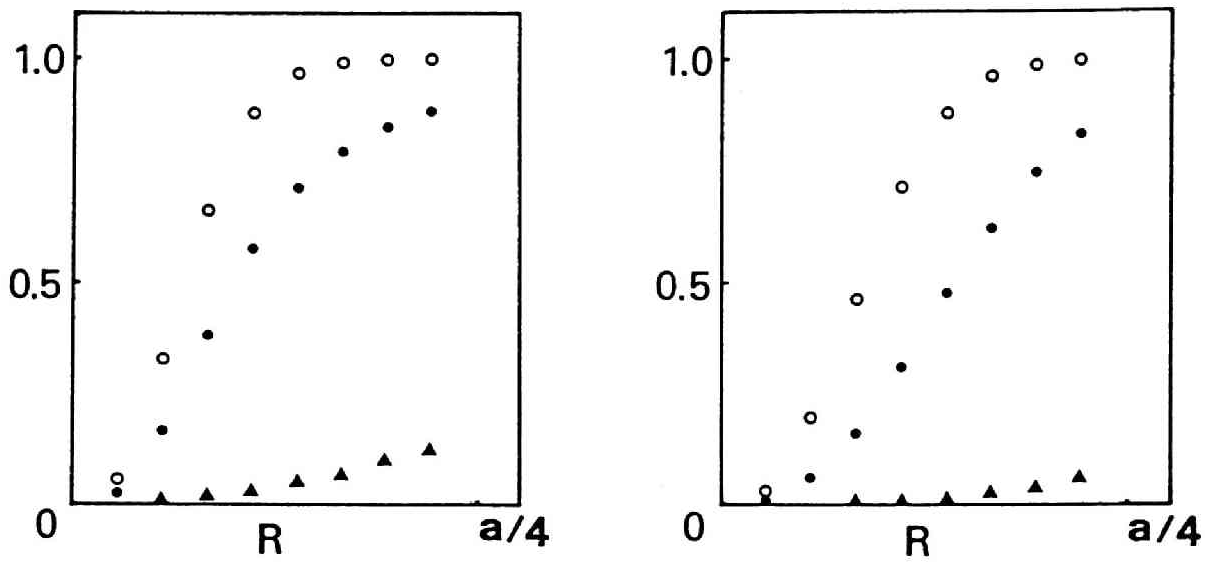

(a) (b)

Fig. 6.4

Fractional number of F^- ions located in spheres at t-site(●) and o-site(▲) as a function of the radius R of the sphere. (a) case A and (b) case C. The results of the same calculation for Ca^{2+} are also plotted for comparison(○).

directions are listed in Table 6.3, where R is taken as $a/10$. The jumps in the <100> direction are more than 80% in both cases. Among these <100> jumps 122 events pass through the inside of spheres at o-sites for A, but only 49 events for C. Thus the diffusion paths for A deflect towards o-sites compared with those for C. In both cases the average flight time, the time F^- spends between the spheres at t-sites (1.12ps for A and 1.15ps for C), is much smaller than the mean residence time at t-sites calculated from the jump frequency(6.16ps for A and 7.66ps for C). Therefore F^- does not *stay* in o-sites even for A, but only *pass* near the o-sites.

Such a difference in the diffusion paths between A and C is considered to be caused by the difference in the softness of the repulsion between F^- and Ca^{2+}. The midpoint of nearest neighbor t-sites is located at the edge of the tetrahedron in the Ca^{2+}-sublattice. The soft-core repulsion between Ca^{2+} and F^- may be large when F^- passes through this point. If n is large, the diffusing F^- is pushed towards the empty o-sites by the strong soft-core repulsion from Ca^{2+}. As a result, the diffusion paths largely deflect towards o-sites when n is 12. However, irrespective of the values of n, more than 80% of F^--jumps occur in the <100> direction, which is the same result as that of earlier MD works.[71-74]

	<100>	<110>	<111>	other direction	total
A	273(80)	55(16)	11(3)	3	342
C	278(84)	47(14)	4(1)	1	330

Table 6.3

The number of jump events in <100>, <110> and <111> directions. The percentages of respective directions are also shown in parenthesis.

CHAPTER VII

DYNAMICS OF DIFFUSION IN CaF_2

7.1 Introduction

As is shown in chapter Ⅵ, F^- diffuses by discrete hops between t-sites irrespective of the difference in the softness of the repulsion. The number of t-sites is the same as that of F^- ions. This is quite different from the case of α-AgI, where the number of t-sites is larger than that of Ag^+ ions. Furthermore, the characteristics of the interionic potential of CaF_2 are different from those of α-AgI. In our simulation σ_F is taken to be equal to σ_{Ca}, whereas σ_{Ag} must be smaller than σ_I for the stability of the I^--sublattice. From these facts, the mechanism of the diffusion in CaF_2 is expected to be different from that in α-AgI.

In this chapter we study the dynamical properties of CaF_2 in comparison with those of α-AgI. The local correlation between F^- and TH's in the Ca^{2+}-sublattice is investigated in the same manner as in α-AgI. The correlated jumps of F^- is studied in detail. A new mechanism of the F^--diffusion is suggested. We also study the vibrational motions by both the VAF's and the dynamical structure factors. In contrast with α-AgI, mobile F^- ions oscillate with higher frequencies than the Ca^{2+}-sublattice.

We analyze the data of the case C at T=1681K presented in chapter Ⅵ. The integration is extended up to $30000\Delta t$. In the analysis of the lattice vibrations we also use the data of the 768-ion system simulated with the same potential

parameters up to 300000Δt. The average temperature and the diffusion constant of the 768-ion system are 1752K and $3.7\times10^{-5}cm^2/sec$, respectively.

7.2 Diffusion of F^- among TH's in the Ca^{2+}-sublattice

Here we apply the analysis concerning TH's to CaF_2. In CaF_2 the Ca^{2+} fcc lattice consists of both TH's and octahedrons(OH's). Since each TH and the adjacent OH have a common face, the diffusion occurs through the face of a TH by way of an OH. Among 278 jump events listed in Table 6.3, we use the 266 events in the following analyses, excluding F^- ions which perform an oscillatory motion near the face of a TH. The instants t_1 and t_2, at which F^- leaves a TH and enters another TH, respectively, of all samples are cataloged. The time $t_0=t_2-t_1$ distributes less than ~0.4ps with the average 0.22ps. This average time is much smaller than the flight time obtained by referring to the spheres. The following quantities at t_1 and t_2 are calculated for Ca^{2+} ions of k and l , which form a common edge of adjacent two TH's. That is,

$$P_{kl} = |r_k - r_l|/a_0, \tag{7.1}$$

and

$$R_{kl} = \frac{1}{2}\frac{d}{dt}(r_k - r_l)^2/a_0 v, \tag{7.2}$$

where $v=(3k_BT/m_{Ca})^{1/2}$ and a_0 is the nearest neighbor distance

between Ca^{2+} ions. The averaged values of P_{kl} at t_1 and t_2 are 1.033 and 1.036, respectively. This means that the common edge is about 3% elongated than a_0 at these instants. The average $\langle R_{kl} \rangle$ is positive(0.055) at t_1 and negative(-0.033) at t_2, which shows that the length of the common edge increases at t_1 and decreases at t_2. These facts suggest that TH's deform so as to make the diffusion easier. This is the same feature as in case of α-AgI.

In order to examine characteristic roles of the Coulomb and soft-core forces separately, we calculate the potential energy experienced by F^- when it leaves and enters TH's. We use 186 samples of F^- trajectories, of which flight time is less than $100\Delta t$. For individual samples, the potential energy curves for F^- at a given instant are calculated by integrating the forces along the trajectories. In case of leaving TH, four specific times $t=t_1-10\Delta t$, t_1, $t_1+10\Delta t$ and $t_1+20\Delta t$ are selected, while in case of entering TH, $t=t_2-20\Delta t$, $t_2-10\Delta t$, t_2 and $t_2+10\Delta t$ are selected. The partial potential energy curves, which are obtained by averaging over the samples, are shown in Fig.7.1(a) for case of leaving and in Fig.7.1(b) for case of entering. All the curves are drawn as a function of time for the time interval $30\Delta t$ and the positions of the circles indicate the instants mentioned above. This is the same calculation as that in Fig.4.2 except that the potential at the initial position is taken as zero.

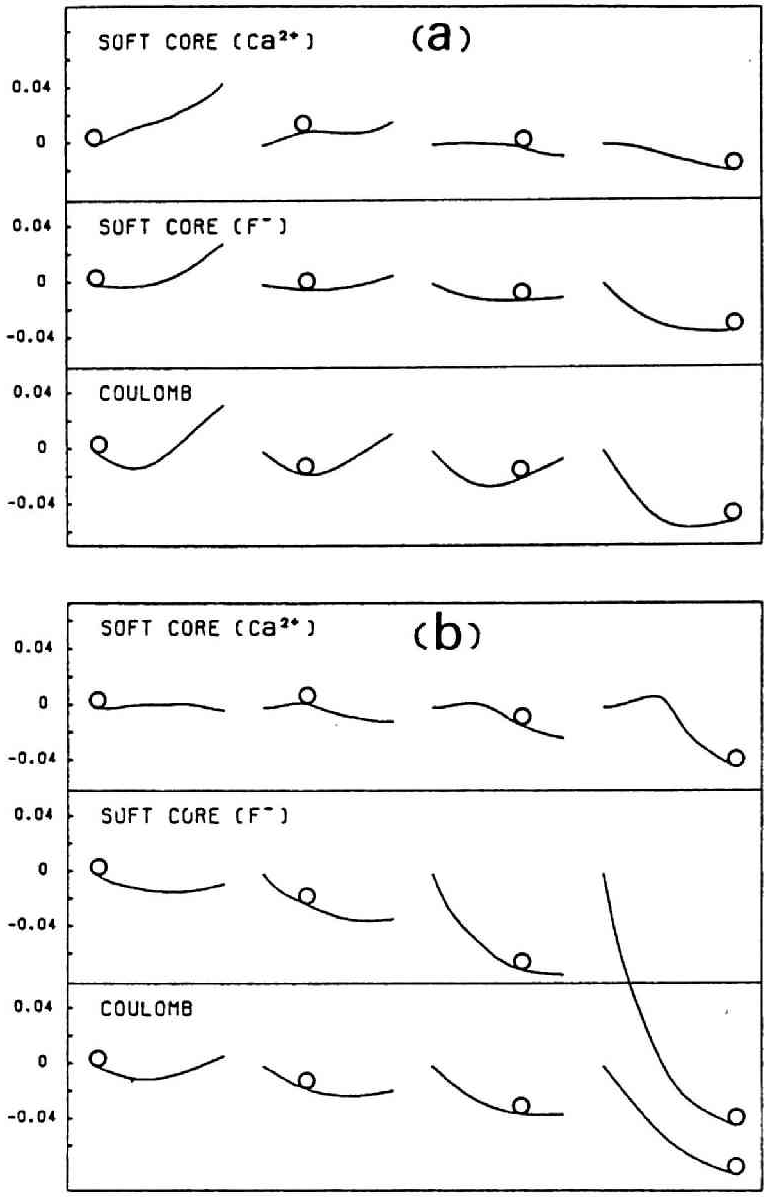

Fig. 7.1

Average potential energy experienced by diffusing F^- along the path for $30\Delta t$. The contributions of repulsions from Ca^{2+} and other F^-, and of Coulomb interactions are shown separately from top. Circles in (a) indicate the positions at $t_1-10\Delta t$, t_1, $t_1+10\Delta t$ and $t_1+20\Delta t$ from left, and in (b) $t_2-20\Delta t$, $t_2-10\Delta t$, t_2 and $t_2+10\Delta t$ from left. The unit of energy is $e^2/\text{Å}$.

The soft-core potential barrier made by Ca^{2+} ions becomes lower when F^- leaves a TH, corresponding to the fact that $\langle R_{kl} \rangle$ is positive at t_1. When F^- enters a TH, there is a small barrier just before t_2 and after that the repulsive force of Ca^{2+} acts so as to push F^-. This feature is more prominent than observed in α-AgI. The variation of Coulomb potential is qualitatively similar to that of α-AgI. The Coulomb force works so as to drive the F^--diffusion when it leaves and enters TH.

An important difference between the present results and those of α-AgI lies in the characteristics of the repulsive force between mobile ions. In Fig.7.1 the soft-core force between F^- ions works to drive the diffusion at all times of the movement. Especially at the time of entering TH, the strong repulsive force acts on the diffusing F^-. This is considered to arise from the interaction with the adjacent F^- which moves in the same direction as the diffusing F^-. These facts suggest that the F^--F^- repulsive force plays an important role for diffusion together with the Coulomb interaction.

7.3 Correlated jumps of F^-

Because all t-sites are occupied by F^- ions, a strong correlation is expected among the jumps of adjacent F^- ions. An example of the trajectories of diffusing F^- ions is shown in Fig.7.2. A jump of F^- always accompanies jumps of neighboring F^- ions. Such a correlation was pointed out in the MD work of Dixon and Gillan,[72,74] who represented the correlated jumps in CaF_2 and $SrCl_2$ diagrammatically.

In order to represent the correlation quantitatively, we calculate the displacement-displacement correlation function of neighboring F^- ions, defined as

$$d_n(t) = \langle (x_{r+n}(t+t_0)-x_{r+n}(t_0))(x_r(t+t_0)-x_r(t_0)) \rangle, \qquad (7.3)$$

where $x_r(t)$ and $x_{r+n}(t)$ are the x-coordinates of F^- ions which are closest to t-site r and its nth neighbor t-site at time t, respectively. The average $\langle\ \rangle$ is taken over the initial time t_0 and over all F^- ions. The function (7.3) is expected to be large when two F^- ions at sites r and $r+n$ diffuse in the same direction and at the same time. The geometrical situation of the sites r and $r+n$ is illustrated in Fig.7.3(a). We denote the direction in which we calculate the displacement as the x-direction. In the figure, n=0 corresponds to the site r , and n=1,2 and 3 correspond to the first, second and third neighbor sites, respectively, in

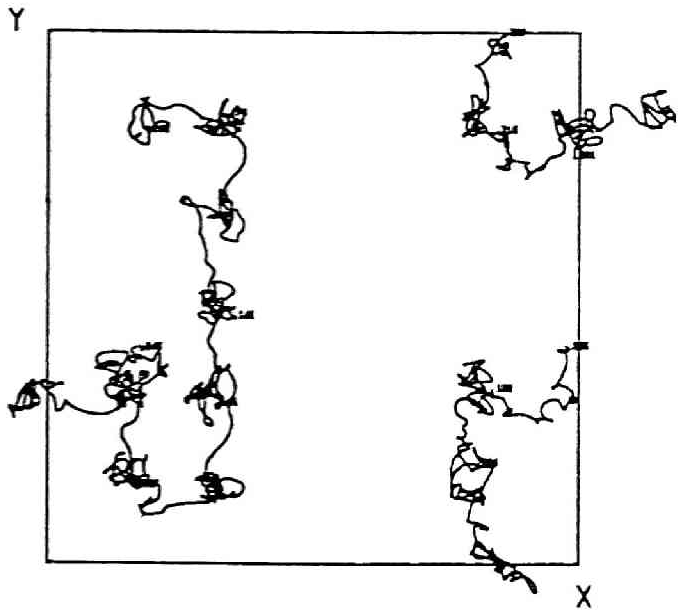

Fig. 7.2

An example of the trajectories of diffusing F^- ions drawn in the same way as in Fig.6.3.

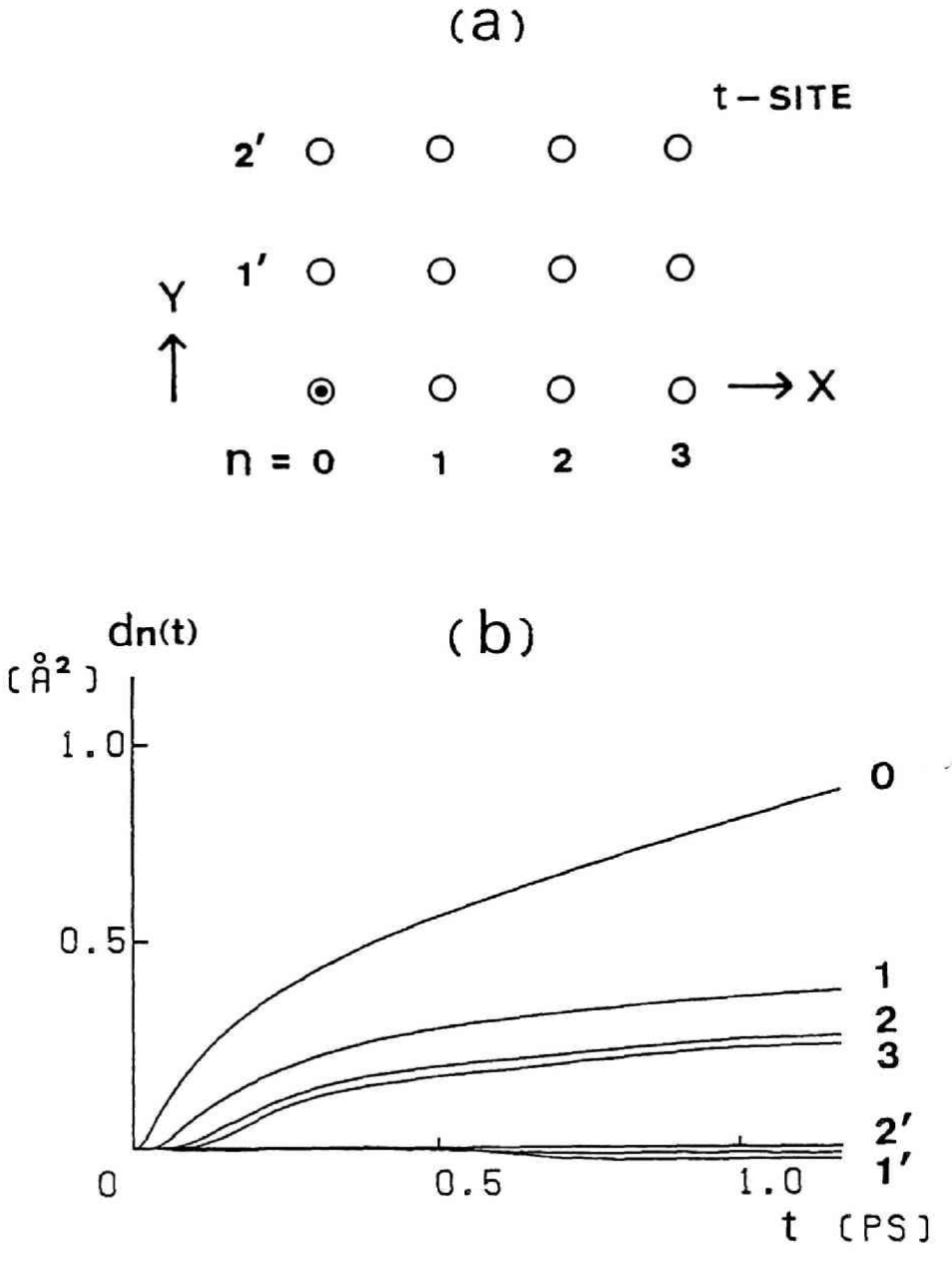

Fig. 7.3

(a) Geometrical relation of the t-sites used in the calculation of $d_n(t)$. (b) Displacement-displacement correlation functions of F^-.

the x-direction. The first and second neighbors in the y-direction perpendicular to the x-direction are denoted as 1' and 2', respectively. The calculated $d_n(t)$ for respective n is shown in Fig.7.3(b). For n=1, 2 and 3 $d_n(t)$ increases with time, but does not for n=1' and 2'. The correlations are observed even with the second and third neighbor ions in the <100> direction. Thus the diffusion occurs mainly by <100> hops accompanying the correlated jumps of neighboring F^- aligned in the direction of diffusion.

Let us investigate the characteristics of the correlated jumps in more detail. We pick out the jumps between t-sites in the same manner as in chapter Ⅵ. That is, the jump between sites is identified as the movement of F^- from a sphere at t-site to the adjacent sphere. Here we take the radius of the sphere as $a/10$. When we get a jump from the site n to the site m, we search for the jump of another F^- from the site m. In this way we follow the sequence of successive jumps. We find that some sequences of jumps form a closed loop. Most of the loops are made up of 4~8 jumps.

Figure 7.4(a) shows the flight time of jumps in the sequence of four jumps. The lateral axis shows time and F^- ions are numbered as 132, 222, 152 and 224. The arrows show the flight time from a sphere to the next one. The figures at both ends of the arrow stand for the numbers of the t-sites before and after the movement. In Fig.7 4(a) we find two types of motions of F^- ions The F^- of 132 departs from the

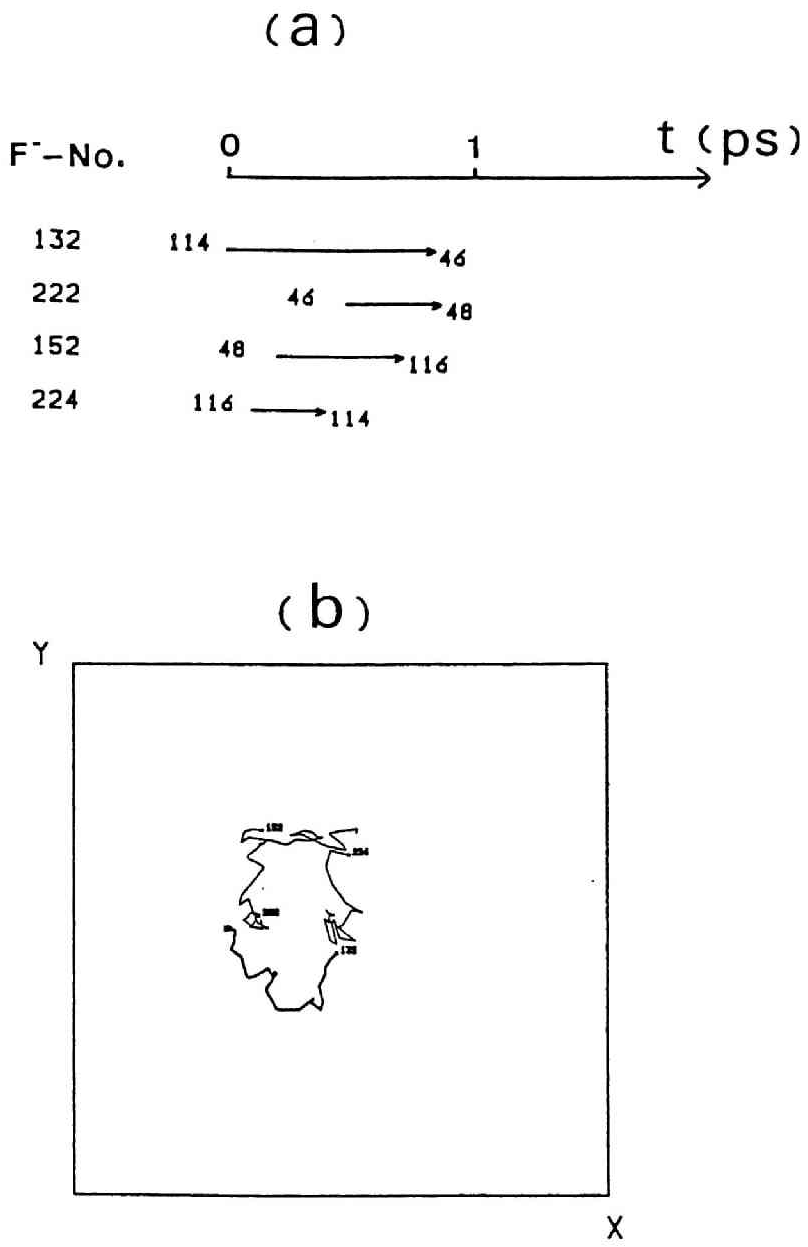

Fig. 7.4

(a) The flight times of four ions. Figures at both ends of arrows show the numbers of *t*-sites. (b) Trajectories of the ions shown in (a), where F^- of 132 is distinguished by a bold line.

t-site 114 for a long time and the F^- ions of 222, 152 and 224 move between t-sites in a rather short time. The trajectories of these F^- ions are drawn in Fig.7.4(b), where the F^- of 132 is identified by the bold line. The motion of F^- of 132 is clearly different from another F^- ions. This suggests that the large motion of the F^- 132 induces the movements of other F^- ions.

7.4 Lattice vibrations

In this section we study the vibrational properties of CaF_2. Figure 7.5 shows the frequency spectra of the VAF's of Ca^{2+} and F^- of the 768-ion system. The spectrum of F^- extends from low frequency($\sim 22ps^{-1}$) to high frequency($\sim 66ps^{-1}$). On the other hand, the Ca^{2+}-spectrum has a large peak at $\omega \sim 22ps^{-1}$ with a bump near the plasma frequency $\omega_p = 83.4ps^{-1}$. This figure is in contrast with that of α-AgI shown in Fig.5.4. The characteristics of the mobile and immobile ion spectra are opposite to those of α-AgI. The spectrum of the Ca^{2+}-sublattice is similar to that of mobile Ag^+ and that of mobile F^- is similar to that of the I^--sublattice. Such a difference is also reflected in collective motions. Figure 7.6 shows the partial dynamical structure factors of Ca^{2+} and F^- in [100] direction calculated in the same manner as in chapter V. Although $\overline{S}_{FF}(\mathbf{k},\omega)$ is similar to $\overline{S}_{CaCa}(\mathbf{k},\omega)$ for small wave vectors, the peaks of the high frequency mode exists in $\overline{S}_{FF}(\mathbf{k},\omega)$ for larger wave vectors. This is also in contrast with the results of α-AgI shown in Fig.5.3. Therefore in CaF_2 mobile F^- ions oscillate at higher frequencies than the Ca^{2+} ions.

Let us investigate the origin of this difference. Recently Kobayashi *et al.*[77] performed the MD simulation of the superionic conductor α-Ag_2Te assuming the potential (1.2) with the parameters similar to our values of α-AgI. α-Ag_2Te

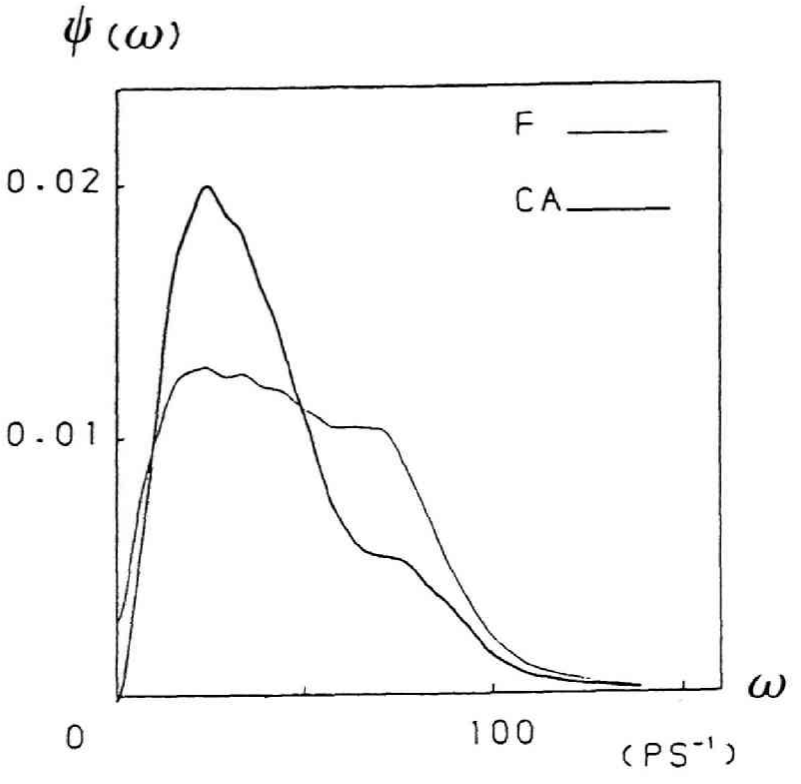

Fig. 7.5

Frequency spectra of Ca^{2+} and F^{-}.

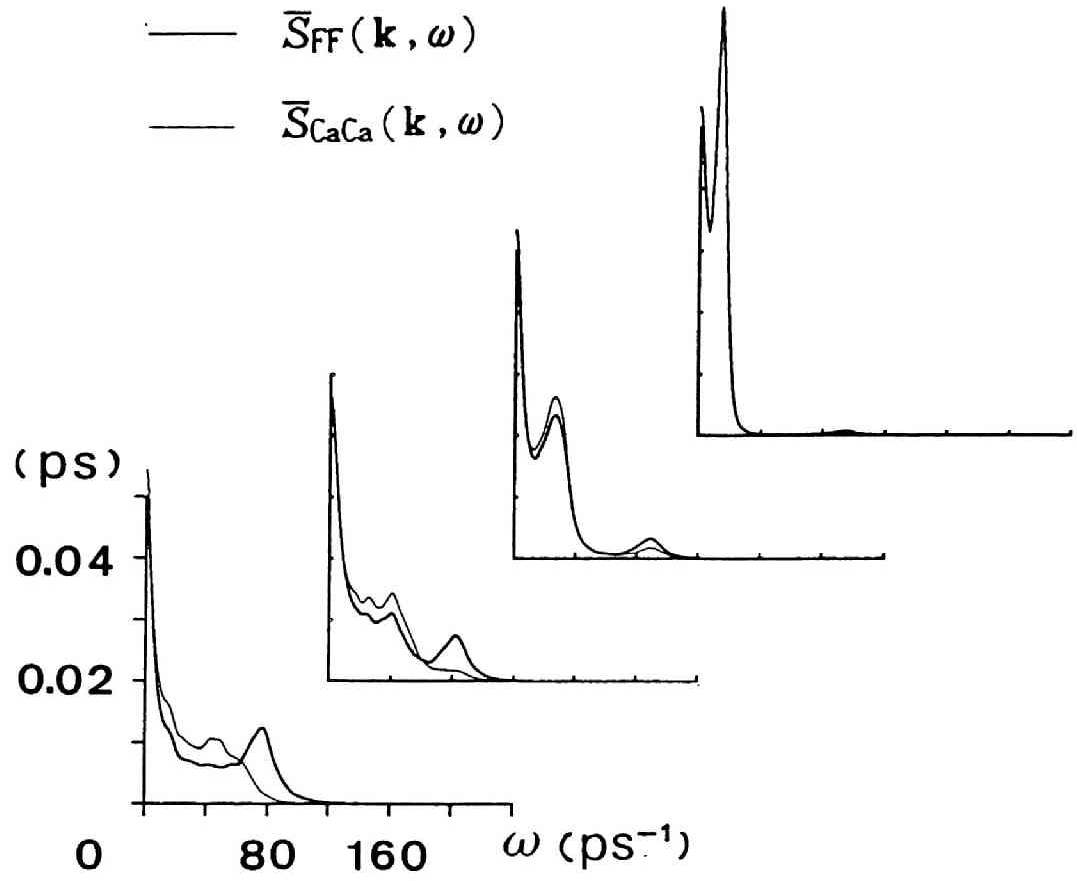

Fig. 7.6

Partial dynamical structure factors of Ca^{2+} and F^- for $\mathbf{k}=(2\pi/a)(\zeta,0,0)$ with ζ=0.25, 0.5, 0.75 and 1.0 from top.

has an anti-fluorite structure, that is, the same structure as CaF_2 except that the roles of cation and anion are interchanged. They showed that the spectra of mobile(Ag^+) and immobile(Te^{2-}) ions are similar to the respective spectra of α-AgI, but not to those of CaF_2. This implies that for vibrational properties the difference in potentials is more significant than that in lattice structures. Here we pay attention to the differences in the ratio of masses and the ratio of core radii. The mass ratios in α-AgI and CaF_2 are $m_{Ag}/m_I=0.85$ and $m_F/m_{Ca}=0.474$. It is reasonable that light F^- ions oscillate with high frequencies. It should be noted that I^- ions oscillate with higher frequencies than light Ag^+ ions. The ratios of core radii are taken as $\sigma_{Ag}/\sigma_I=0.28$ and $\sigma_F/\sigma_{Ca}=1.0$ in our simulations. In α-AgI the repulsive force between I^- ions is much stronger than that between silver ions. However, since σ_F/σ_{Ca} is taken as unity, a one-component like structure of the Ca^{2+}-spectrum can not be expected in CaF_2.

In order to see the influence of the parameters we have performed the following calculations. In the simulation of CaF_2, we replace σ_F/σ_{Ca} and/or m_F/m_{Ca} by the values of α-AgI and compare the spectra of the VAF's. The results are summarized in Fig.7.7. Figure 7.7(a) shows the spectra of the original CaF_2. Figure 7.7(b) shows the case in which σ_F/σ_{Ca} is taken as 0.28 and in Fig.7.7(c) m_F/σ_{Ca} is taken as 0.85 In Fig.7.7(d) both σ_F/σ_{Ca} and m_F/m_{Ca} are changed. The

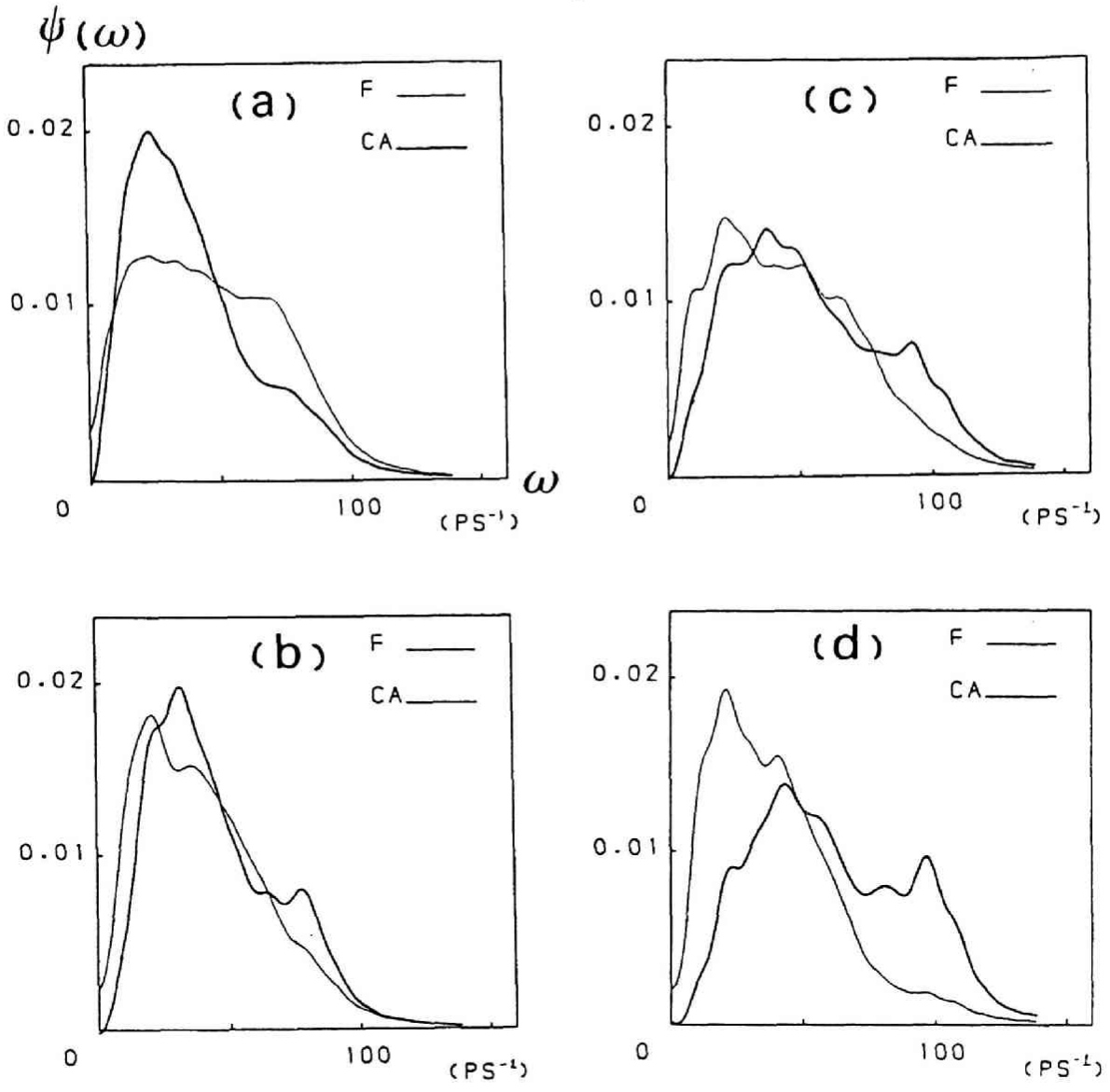

Fig. 7.7

Dependence of the frequency spectra of VAF's on the ratio of masses and the ratio of core radii.

(a) The spectra of CaF_2

(b) σ_F/σ_{Ca} is replaced by the value of AgI.

(c) m_F/m_{Ca} is replaced by the value of AgI.

(d) Both σ_F/σ_{Ca} and m_F/m_{Ca} are replaced.

average temperatures of the states shown in Fig.7.7(b), (c) and (d) are 1664K, 1618K and 1688K, respectively, and the diffusion constants of F^- are 2.77×10^{-5}, 2.17×10^{-5} and 2.4×10^{-5}[cm^2/s], respectively. In each state the Ca^{2+}-sublattice is stable. The peak at a high frequency appears in the Ca^{2+}-spectrum in Fig.7.7(b) and (c), which means that both the ratio of masses and the ratio of core radii contribute to the difference in the spectra. Fig.7.7(d) quite resembles the spectra of α-AgI. This clearly shows that the difference in the spectra is attributed to the differences in the ratio of masses and in the ratio of core radii.

7.5 Summary

The main results on the dynamics of CaF_2 are summarized as follows.

(1) When F^- diffuses between TH's by way of an OH, TH's deform so as to make the movement easier, which is the same result as in α-AgI. The soft-core force between F^- ions is important for the diffusion as well as the Coulomb interaction.

(2) The diffusion of F^- occurs by the correlated jumps between t-sites. The correlation of mobile ions is also observed in α-AgI (Fig.4.6(b)), but it is more prominent in CaF_2. There observed two types of motions of diffusing F^- ions. Some F^- departs largely from t-sites and the surrounding F^- ions move between t-sites in a rather short time.

(3) The vibrational motion of CaF_2 is quite different from that of α-AgI. Mobile F^- ions oscillate with higher frequencies than the immobile Ca^{2+} ions. This is due to the difference in the ratio of masses and the ratio of core radii.

The result (2) is considered as a clue to understand the mechanism of correlated jumps. The motions of F^- ions in the sequence of jumps are not identical. Some F^- departs largely from t-sites and seems to induce the jumps of surrounding F^- ions. Figure 7.8 shows an example of a long sequence of jumps drawn in the same way as Fig.7.4(a). We can observe the two types of motions discussed above. The

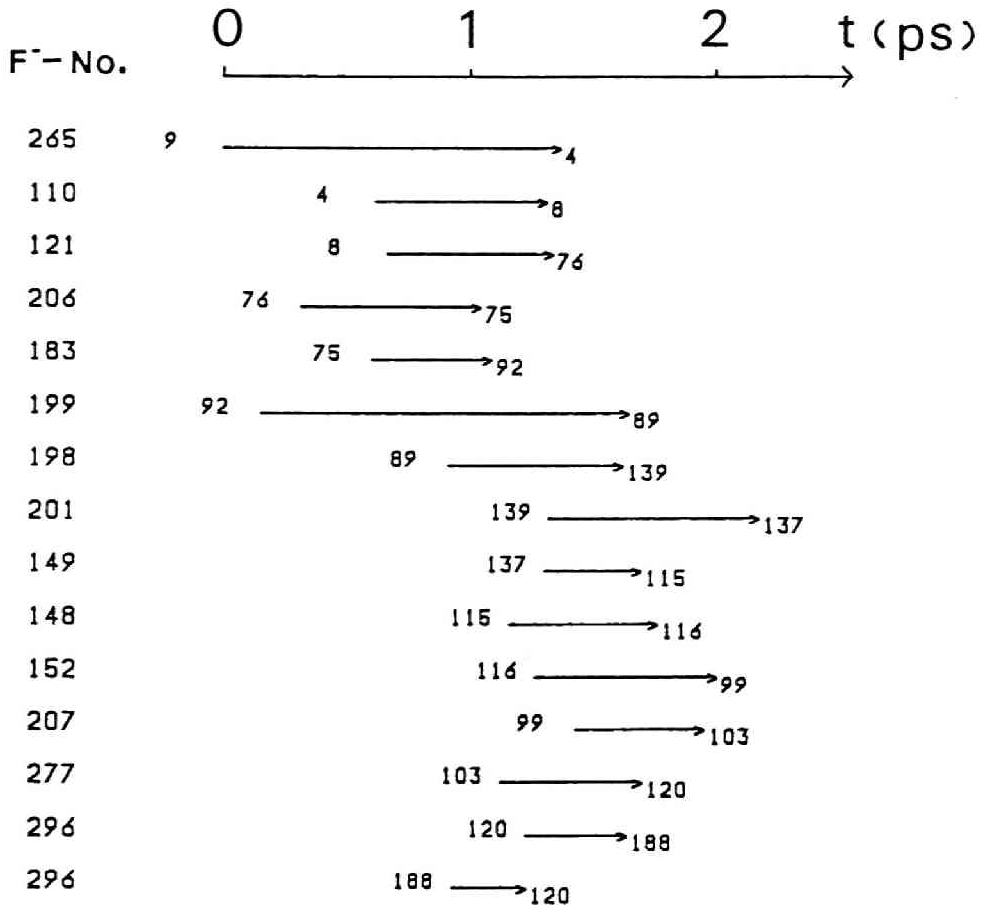

Fig.7.8

Flight times of diffusing F^- ions in a long sequence of correlated jumps drawn in the same way as in Fig.7.4.

large motion is always followed by the jumps with a short flight time. This is considered as the general feature of the correlated jumps in CaF_2.

CHAPTER VII

CONCLUSIONS

Applying the ionic soft-core system, we have studied the ionic motions in superionic conductors in view of two problems mentioned in chapter I. Here we summarize our results comparing α-AgI and CaF_2.

(1) *The characteristics of the interionic potential which give rise to the superionic phase.*

This problem is studied in detail for α-AgI. The ratio σ_{Ag}/σ_I must be appropriately small (< 0.4) and the additivity rule $\sigma_{Ag}+\sigma_I$=n.n.d. is necessary for the stability of the I^--sublattice. The diffusion of Ag^+ ions is necessary to keep the symmetry of the lattice structure, which also contributes to the stability of the I^--sublattice. In order that the diffusion of Ag^+ occurs, the "Coulomb" force must be appropriately weak. One of the origin to reduce the "Coulomb" force is the smallness of the ionicity f, which is related with the partially covalent interaction between Ag^+ and I^-.

In CaF_2 the stability of the lattice is not so sensitive to the interaction potential as in α-AgI. The structure of the Ca^{2+}-sublattice is stable in all simulated states presented in this paper, where the condition $\sigma_{Ca}+\sigma_F$=n.n.d. is satisfied. This implies that the stability of a loosely packed structure is more sensitive to the potential than that of a closely-packed structure. The distribution of F^- ions in the superionic phase is not influenced by the softness of

the repulsive potential. Irrespective of the value of n, F^- occupies t-sites and moves between sites. The diffusion path, however, is influenced by the potential. The path between t-sites largely deflects towards octahedral positions when the soft-core repulsion becomes harder.

(2) *The dynamic correlation and the mechanism of diffusion.*

In α-AgI Ag^+ ions behave quite liquid-like through the cage of the I^--sublattice. This is clearly observed in the 16mm movie. Ag^+ oscillates rather slowly in a TH coupled with the low frequency LA mode at long wavelengths. TH's oscillate in a high frequency LO mode, which is not correlated with the vibrational motion of Ag^+ ions. When TH's deform so as to lower the soft-core potential barrier, Ag^+ moves smoothly to the adjacent TH. The main driving force is the Coulomb force. The movement of Ag^+ results in the relaxation of the local distortion of the I^--sublattice. This is quite different from the jump diffusion picture usually applied to the diffusion in solids [78]

The jump diffusion picture in CaF_2 so far discussed in earlier works is reconfirmed in our simulation. The diffusion of F^- occurs by discrete hops between t-sites mainly in <100> direction. As in case of α-AgI, when F^- moves between TH's by way of an OH, TH's deform so as to make the movement easier The F^--F^- repulsive force is important for the diffusion as well as the Coulomb force. The vibrational

property of CaF_2 is quite different from that of α-AgI. Mobile F^- ions oscillate with higher frequencies than Ca^{2+} ions. This is attributed to the difference in the ratio of masses and the ratio of core radii.

The diffusion in CaF_2 is characterized as the "correlated jumps". A sequence of the jumps of F^- ions aligned in <100> direction is clearly observed. We represented the correlation quantitatively by the displacement-displacement correlation function. A new mechanism of the correlated motions is suggested. As is shown in Figs 7.4 and 7.7, some F^- moves largely out of t-sites. The jumps of neighboring F^- ions seem to be induced by the large motion. This diffusion mechanism seems different from that so far discussed in the literatures.[5-8)]

REFERENCES

1) C.Tubandt and F.Lorentz : Z.Phys.Chem. 87 (1914) 513.

2) L.W.Strock : Z.Phys.Chem. 25 (1934) 411.

3) P.Rahlfs : Z.Phys.Chem. 31 (1936) 156.

4) Y.F.Y.Yao and J T.Kummer : J.Inog.Nucl.Chem. 29 (1967) 2453.

5) *Superionic Conductors*, ed. G.D.Mahan and W.L.Roth, (Pleunm, New York, 1976).

6) *Solid Electrolytes*, ed. P.Hagenmuller and W van Gool, (Academic Press, 1978)

7) *Physics of Superonic Conductors*, ed. M.B.Salamon, (Springer, 1979).

8) S.Chandra : *Superionic Solids* (North-Holland, 1981).

9) J.B.Boyce and B.A.Huberman : Physics Reports 51 (1979) 189

10) B.A.Huberman and R.M.Martin : Phys.Rev.B 13 (1976) 1498.

11) H.Hinkelmann and B.A.Huberman : Solid State Commun. 19 (1976) 365.

12) I.Yokota : J.Phys.Soc.Jpn. 21 (1966) 420

13) for example, W.Dieterich, P.Fulde and I.Peschel : Advances in Physics 29 (1980) 527

14) P.Fulde, L.Pietronero, W.Shneider and S.Strässler : Phys.Rev.Lett 35 (1975) 1776.

15) H.Mori : Prog.Theor.Phys 34 (1965) 399

16) W.Bührer, R.M.Nicklow and P.Brüesch : Phys.Rev.B17 (1978) 3362.

17) R.Alben and G.Burns : Phys.Rev.B 16 (1977) 3748.

18) *Molecular Dynamics Simulation of Statistical Mechanical Systems*, ed. G.Ciccotti and W.G.Hoover, (North-Holland, Amsterdam, 1985).

19) B.J.Alder and T.E.Wainwright : J.Chem.Phys. 31 (1959) 459. ; *ibid.* 33 (1960) 1439. ; Phys.Rev. 127 (1962) 359.

20) A.Rahman : Phys.Rev. 136 (1964) A405. ; Phys.Rev. Lett. 19 (1967) 420.

21) A.Rahman : Phys.Rev.Lett. 32 (1974) 52. ; Phys.Rev.A 9 (1974) 1667.

22) L.Verlet : Phys.Rev. 159 (1967) 159. ; *ibid.* 165 (1968) 201.

23) D.Levesque and L.Verlet : Phys.Rev.A 2 (1970) 2514.

24) D.Levesque, L.Verlet and J.Kürkijarvi : Phys.Rev.A 7 (1973) 1690.

25) J.P.Hansen, I.R.McDonald and E.L.Pollock : Phys.Rev.A 11 (1975) 1025.

26) J.P.Hansen and I.R.McDonald : Phys.Rev.A 11 (1975) 2111.

27) J.R.D.Copley snd A.Rahman : Phys.Rev.A 13 (1976) 2276.

28) E.M.Adams, I.R.McDonald and K.Singer : Proc.R.Soc.A 357 (1977) 37.

29) E.R.Cowley, G.Jacucci, M.L.Klein and I.R.McDonald : Phys.Rev.B 14 (1976) 1758.

30) J.P.Hansen, I.R.McDonald and P.Vieillefosse : Phys.Rev.A 20 (1979) 2590.

31) R.J.Cava, F.Reidinger and B.J.Wuensch : Solid State Commun. 24 (1977) 411.

32) M.H.Dickens, W.Hayes, P.Schnabel, M.T.Hutchings, R.E.Lechner and B.Renker : J.Phys.C 16 (1983) L1.

33) M.T.Hutchings, K.Clausen, M.H.Dickens, W.Hayes, J.K.Kjems, P.G.Schnabel and C.Smith : J.Phys.C 17 (1984) 3903.

34) W.G.Hoover, D.A.Young and R.Grover : J Chem Phys. 56 (1972) 2207.

35) Y.Hiwatari and H.Matsuda : Prog.Theor.Phys. 47 (1972) 741

36) Y.Hiwatari, H.Matsuda, T.Ogawa, N.Ogita and A.Ueda : Prog.Theor.Phys. 52 (1974) 1105.

37) Y.Hiwatari and A.Ueda : J.Phys.Soc.Jpn. 48 (1980) 766.

38) Y.Hiwatari and A.Ueda : J.Phys.Soc.Jpn. 49 (1980) 2129.

39) A.Fukumoto, A.Ueda and Y.Hiwatari : Solid State Ionics 3/4 (1981) 115.

40) A.Fukumoto, A.Ueda and Y.Hiwatari : J.Phys.Soc.Jpn. 51 (1982) 3966

41) M.Hokazono, A.Ueda and Y.Hiwatari : Solid State Ionics

13 (1984) 151.

42) L.Verlet : Phys.Rev. 159 (1967) 98.

43) M.J.L.Sangster and M.Dixon : Advances in Physics 25 (1976) 247.

44) S.Hoshino, T.Sakuma and Y.Fujii : Solid State Commun. 22 (1977) 793.

45) J.B.Boyce, T.M.Hayers, W.Stutius and J.C.Mikkelsen : Phys.Rev.Lett. 38 (1977) 1362.

46) W.Schommers : Phys.Rev.Lett 38 (1977) 1536. ; Phys.Rev.B 17 (1978) 2057. ; *ibid.* 21 (1980) 847.

47) P.Vashishta and A.Rahman : Phys.Rev.Lett. 40 (1978) 1337. ; in *The Physics of Superionic Conductors and Electrode Materials*, ed. J.W.Perram, (Plenum, 1983) 93

48) L.Pauling : *The Nature of the Chemical Bond* (Cornell Univ. Press, Ithaca, New York, 1960).

49) J.M.Dickey and A.Paskin : Phys.Rev. 188 (1969) 1407.

50) A.Kvist and R.Tärneberg : Z.Naturforsch. 25A (1970) 257.

51) R.E.Lechner : in *Mass Transport in Solids* , ed. F.Beniere and C.R.A.Catlow (Plenum Press, New York and London, 1981) 169.

52) C.T.Chudley and R.J.Elliott : Proc.Phys.Soc. London 77 (1961) 353.

53) J.R.D.Copley and J.M.Rowe : Phys.Rev.Lett. 32 (1974) 49.

54) W.E.Alley, B.J.Alder and S.Yip : Phys.Rev.A 27 (1983)

3174.

55) J.P.Hansen and M.L.Klein : Phys.Rev.B 13 (1976) 878.

56) H.R.Glyde, J.P.Hansen and M.L.Klein : Phys.Rev.B **16** (1977) 3476.

57) G.Jacucci, M.L.Klein and R.Taylor : Phys.Rev.B **18** (1978) 3782.

58) G.Jacucci and M.L.Klein : Phys.Rev.B 16 (1977) 1322.

59) S.W.de Leeuw : Mol.Phys. **37** (1979) 489.

60) G.Eckold, K.Funke, J.Kalus and R.E.Lechner : J.Phys.Chem.Solids 37 (1976) 1097.

61) for example, W.Cochran : *The Dynamics of Atoms in Crystals* (Crane, Russak New York, 1973).

62) P.Brüesch, W.Bührer and H.J.M.Smeets : Phys.Rev.B 22 (1980) 970.

63) R.Zeyher : Z.Phys.B **31** (1978) 127.

64) H.Mori : Prog.Theor.Phys. 33 (1965) 423.

65) C.R.A.Catlow and M.J.Norgett : J.Phys C 6 (1973) 1325

66) C.R.A.Catrow, M.J.Norgett and T.A.Ross : J.Phys.C 10 (1977) 1627

67) K.Koto, H.Schulz and R.A.Huggins : Solid State Ionics 1 (1980) 355.

68) K.Koto, H.Schulz and R.A.Huggins : Solid State Ionics 3/4 (1981) 381

69) A.Rahman : J.Chem.Phys. 65 (1976) 4845

70) Y.S.Kim and R.G.Gordon : J.Chem.Phys. 60 (1974) 4332.

71) G.Jacucci and A.Rahman : J.Chem.Phys. 69 (1978) 4117.

72) M.Dixon and M.J.Gillan : J.Phys.C 11 (1978) L165.

73) M.J.Gillan : J.Phys.C 19 (1986) 3391 and 3517.

74) M.J.Gillan and M.Dixon : J.Phys.C 13 (1980) 1901 and 1919. ; J.Phys.C : 13 (1980) L835.

75) A.Rahman : in *Fast Ion Transport in Solids* ed. P.Vashishta, J.N.Mundy and G.K.Shenoy (Elsevier North-Holland, 1979) 643.

76) W.G.Hoover, S.G.Gray and K.W.Johnson : J.Chem.Phys. 55 (1971) 1128.

77) M.Kobayashi, K.Ishikawa, F.Tachibana and H.Okazaki : Phys.Rev.B 38 (1988) 3050.

78) *Diffusion in Solids*, ed. A.S.Nowick and J.J.Burton (Academic Press, 1975).

LIST OF PUBLICATIONS

1. A. Ueda and Y. Kaneko : Butsuri 40 No.11 (1985) 866.
   "Superionic Conductor - Stability of Sublattice and Dynamic structure - "
   (in Japanese)

2. Y. Kaneko, A. Ueda and Y. Hiwatari : J.Phys.Soc.Jpn. 55 (1986) 1244.
   "Superionic Conductivity and Interionic Potential"

3. Y. Kaneko and A. Ueda : J.Phys.Soc.Jpn. 55 (1986) 3924.
   "Dynamic Correlation and Cation Diffusion in α-AgI"

4. Y. Kaneko and A. Ueda : J.Phys.Soc.Jpn. 57 (1988) 3064.
   "Molecular Dynamics Studies of Superionic Conductor CaF_2"

5. Y. Kaneko and A. Ueda : Phys.Rev.B 39 (1989).
   "Dynamical Structure Factor of α-AgI"